This is the accepted manuscript made available via CHORUS. The article has been published as:

Resolution-induced anisotropy in large-eddy simulations

Sigfried W. Haering, Myoungkyu Lee, and Robert D. Moser

Phys. Rev. Fluids **4**, 114605 — Published 13 November 2019

DOI: 10.1103/PhysRevFluids.4.114605

Resolution-induced anisotropy in LES

Sigfried W. Haering and Myoungkyu Lee
The Oden Institute for Computational Engineering and Science,
The University of Texas at Austin

Robert D. Moser
Department of Mechanical Engineering,
The Oden Institute for Computational Engineering and Science,
The University of Texas at Austin
(Dated: October 5, 2019)

Large eddy simulation (LES) of turbulence in complex geometries and domains is often conducted with high aspect ratio resolution cells of varying shapes and orientations. The effects of such anisotropic resolution are often simplified or neglected in subgrid model formulations. Here, we examine resolution induced anisotropy and demonstrate that, even for isotropic turbulence, anisotropic resolution induces mild resolved Reynolds stress anisotropy and significant anisotropy in second-order resolved velocity gradient statistics. In large eddy simulations of homogeneous isotropic turbulence with anisotropic resolution, it is shown that commonly used subgrid models, including those that consider resolution anisotropy in their formulation, perform poorly. The one exception is the anisotropic minimum dissipation model proposed by Rozema *et al.* (*Phys. of Fluids* **27**, 085107, 2015). A simple new model is presented here that is an anisotropic eddy diffusivity extension of the "Kolmogorov expression" eddy viscosity of Carati *et al.* (*CTR Annual Research Briefs*, 1995) that depends explicitly on the anisotropy of the resolution. It also performs well, and is remarkable because unlike other LES subgrid models, the eddy diffusivity only depends on statistical characteristics of the turbulence (in this case the dissipation rate), not on fluctuating quantities. In other subgrid modeling formulations, such as the dynamic procedure, limiting flow dependence to statistical quantities in this way could have advantages.

I. INTRODUCTION

The expansion of available computing power has led to an increasing reliance on numerical simulation of complex systems in engineering, science and decision making. With this increased reliance comes a demand for modeling accuracy and reliability in general and specifically in turbulent fluid flows. The increased resolution enabled by advances in computing hardware, and increased numerical accuracy that has arisen from advances in numerical algorithms has improved the reliability of computational models of turbulent flows, but improvements in turbulence models have lagged behind. It has long been expected that large eddy simulation (LES) would address the need for improved modeling fidelity in engineering flows. However, numerous challenges remain before LES can become a robust tool capable of reliable predictions of complex turbulent flows for use in research and development. Since the advent of the dynamic modeling approach [1, 2], wall modeling has been considered the greatest impediment to reliable LES, and this has been the focus of much LES research [3–5]. While this is certainly a critical issue, there are also other challenges. One such is considered here.

In practical flows of engineering interest, the combination of high Reynolds number, complex geometry and limited computational resources often dictates discretization with relatively coarse, highly anisotropic and spatially varying resolution. In such cases, the common assumptions of isotropic unresolved turbulence in equilibrium with the large scales and homogeneous filtering may be violated. For example, use of a scalar eddy viscosity is based on the assumption of isotropic subfilter turbulence. When this assumption is violated, a scalar eddy viscosity model would be expected to produce inaccurate momentum transport and inaccurate transfer of energy from the resolved to unresolved scales, resulting in poor LES predictions. In this work, we focus in particular on the consequences of anisotropic numerical resolution and the associated anisotropic definition of the large and small scales. We will refer to this simply as anisotropic resolution.

Though the issue of anisotropic resolution has been acknowledged in many SGS models [6–8], the validity of SGS models in the presence of anisotropic resolution has not been examined in detail. The use of anisotropic resolution in LES is known to induce "artificial" anisotropy in the resolved and subgrid stress even for the simplest case of isotropic turbulence [9]. In this work, we examine the implications of anisotropic resolution in LES and propose a simple modeling treatment which has potential to be integrated into existing models. Before continuing, we briefly review existing resolution anisotropy treatments in the literature. Some of the models mentioned below are evaluated in Sec. IV.

In most cases, resolution anisotropy has been acknowledged through the definition of a scalar resolved length scale

in terms of anisotropic resolution parameters. This resolved scale is then used in the formulation of subgrid models, such as the Smagorinsky model. However, scalar measures discard all the information about resolution anisotropy. For instance, consider the commonly used cube-root of a cell volume given by $\Delta_{eq} = (\Delta_1\Delta_2\Delta_3)^{1/3}$ [10], where Δ_α are the resolution scales in each direction in an orthogonal grid. This length scale will favor the smallest dimension of the grid and will thus provide an unresolvable model scale in coarse directions. Such a simplification results in LES turbulence that is essentially under resolved in these directions and causing spectral energy pile ups at the resolved scale. Conversely, scalar resolution measures based on the cell diagonal given by $\Delta_{eq} = (\Delta_1^2 + \Delta_2^2 + \Delta_3^2)^{1/2}/\sqrt{3}$ [11], favor the largest dimension of the grid resulting in LES turbulence that is smoother in fine directions than could be resolved. This is essentially a waste of resolution. Further, without explicit filtering corresponding to the cell diagonal scale, the spectral energy distribution will be affected by finer grid scales present. In short, the LES turbulence is inconsistent with the with anisotropic filtering of real turbulence.

The first direct treatment of resolution anisotropy in LES models was proposed by Schumann [12]. In this approach, the subgrid momentum flux through each face of a computational cell was modeled with a different length scale (the face diagonal) and with different model coefficients for each momentum component, to represent the effects of resolution anisotropy. A similar approach was later used by Zahrai *et al* [13], but with anisotropy scaling with the face-normal grid dimension to the 4/3 power and without varying model coefficients. Both methods showed good agreement with data in channel flow, with results being relatively insensitive to resolution anisotropy. However, these anisotropy treatments are intimately linked to the specific discretization employed, thereby severely limiting their potential application.

In an attempt to alleviate under-resolution in coarse directions, Scotti *et.al.* [6] introduced a scalar correction to Δ_{eq} in the standard Smagorinsky model, based on the ratio of the refined to most coarse grid dimensions with the aim of ensuring correct total dissipation. While an improvement over the basic Smagorinsky model because it reduces artifacts of under-resolution in the course directions, it is at the cost of even worse under-utilization of available resolution in the fine directions. It appears that these simple model forms preclude LES that produce spectra consistent with anisotropic resolution.

The Vreman model [7], which was primarily designed to ensure that the eddy viscosity vanishes in laminar regions, was the first to directly consider resolution anisotropy in a discretization agnostic formulation. In this model, the eddy viscosity scales with the square root of the second invariant of the velocity gradient tensor with gradient components weighted by the corresponding grid length scale where the cells are assumed to be aligned with the global coordinate system. The magnitude of the resulting eddy viscosity is reduced in regions where high gradients are aligned with fine resolution directions and vice-versa. However, in the end, resolution anisotropy information is again discarded in favor of maintaining a scalar eddy viscosity. As shown in Sec. IV, the result with anisotropic resolution is similar to Smagorinsky.

Rozema *et al.* have more recently extended minimal dissipation models [14] to account for grid anisotropy (AMD), without making a scalar filter width approximation like that described above [8]. Their model is motivated by the Poncàire inequality applied to anisotropic (rectilinear) grid cells, and is formulated to ensure that the eddy viscosity is sufficient to dissipate energy at the estimated rate of small-scale energy production. Here the anisotropy of the resolution enters into the estimate of the small-scale production. The AMD model performs quite well with anisotropic resolution and it is also examined in some detail in Sec. IV.

Here, we pursue an evaluation of the impact of resolution anisotropy on large eddy simulation models by simulating isotropic turbulence with anisotropic resolution. The subgrid models described above that consider resolution anisotropy, along with Smagorinsky, are evaluated. Furthermore, we develop and evaluate a simple anisotropic tensor eddy viscosity model. The model is particularly simple in that the eddy viscosity does not fluctuate, though it does depend on statistical properties of the turbulence being simulated, in this case the dissipation.

In the remainder of the paper, the characteristics of resolution-induced anisotropies in LES are discussed in Sec. II; our simple anisotropic subgrid model is introduced in Sec. III; and, the performance of subgrid models in isotropic turbulence simulated with anisotropic resolution is explored in Sec. IV. Finally, discussion and conclusions are offered in Sec. V.

II. RESOLUTION-INDUCED ANISOTROPIES

To assess the importance of resolution anisotropy in LES, we begin with a theoretical investigation of the impact on the statistics of the resolved field (Sec. II A). Details of the large eddy simulations used to assess the ability of LES models to treat resolution anisotropy are described in Sec. II B, and the results of such simulations with the Smagorinsky model are presented in Sec. II C.

A. *A Priori* Consequences of Resolution Anisotropy

In a large eddy simulation with anisotropic resolution, the anisotropy of the resolution is expected to produce anisotropy of the resolved and the subgrid turbulent stresses. Of course, in homogeneous isotropic turbulence (HIT), the mean turbulent stress (Reynolds stress) is dynamically insignificant. However, in an LES of HIT with anisotropic resolution, the resolved and subgrid Reynolds stress can be anisotropic, though their sum is still isotropic and homogeneous. To examine how the resolved and subgrid Reynolds stress anisotropies depend on resolution anisotropy, consider an idealized infinite Reynolds number isotropic turbulence with a $|\boldsymbol{\kappa}|^{-5/3}$ inertial range spectrum, where $\boldsymbol{\kappa}$ is the wavevector, starting at minimum wavenumber κ_m. The Reynolds stress anisotropy can be determined by integrating the inertial range energy spectrum over an anisotropic domain of resolved wavenumbers $\mathcal{D}$ [9]. That is, with the velocity decomposed as filtered and subfilter scales, $u = \bar{u} + u'$, the resolved and unresolved Reynolds stresses ($\langle \bar{u}_i \bar{u}_j \rangle$ and $\langle u'_i u'_j \rangle$, respectively) can be found by integrating the velocity-spectrum tensor $\Phi_{ij}(\boldsymbol{\kappa})$ over the resolved wavenumber domain $\mathcal{D}$ and it's compliment. For isotropic turbulence, Φ_{ij} is known in terms of the energy-spectrum function [15], which in the Kolmogorov inertial range is given by $E(|\boldsymbol{\kappa}|) = C_k \varepsilon^{2/3} |\boldsymbol{\kappa}|^{-5/3}$, where ε is the mean dissipation, C_k the Kolmogorov constant and δ_{ij} the Kronecker delta. The resulting resolved and unresolved contributions to the Reynolds stress are:

$$\langle \bar{u}_i \bar{u}_j \rangle = \frac{C_k \varepsilon^{2/3}}{4\pi} \int_{\mathcal{D}} |\boldsymbol{\kappa}|^{-11/3} \left(\delta_{ij} - \frac{\kappa_i \kappa_j}{|\boldsymbol{\kappa}|^2} \right) d\boldsymbol{\kappa} \tag{1}$$

and

$$\langle u'_i u'_j \rangle = \frac{C_k \varepsilon^{2/3}}{4\pi} \int_{\tilde{\mathcal{D}}} |\boldsymbol{\kappa}|^{-11/3} \left(\delta_{ij} - \frac{\kappa_i \kappa_j}{|\boldsymbol{\kappa}|^2} \right) d\boldsymbol{\kappa}, \tag{2}$$

where $\tilde{\mathcal{D}}$ is the domain of unresolved wavenumbers.

In this paper, we consider two anisotropic definitions of the resolved wavenumber domain. The first is an ellipsoidal wavenumber domain, with major axes determined by the cutoff wavenumber $\kappa_{c\alpha} = \pi/\Delta_\alpha$ in each direction, where Δ_α is the Nyquist grid spacing in the α direction. An ellipsoidal wavenumber domain is analogous to the spherical wavenumber cut-off commonly used in LES of isotropic turbulence. Arguably ellipsoidally filtered turbulence is the most meaningful target of an isotropic turbulence LES with anisotropic resolution. The ellipsoidal resolved domain $\mathcal{D}^e$ and the associated domain of unresolved wavenumbers $\tilde{\mathcal{D}}^e$ are given by

$$\begin{aligned} \mathcal{D}^e &= \left\{ \boldsymbol{\kappa} \;\middle|\; \sum_{\alpha=1}^{3} \kappa_\alpha^2 > \kappa_m^2 \quad \text{and} \quad \sum_{\alpha=1}^{3} \left(\frac{\kappa_\alpha}{\kappa_{c\alpha}} \right)^2 \leq 1 \right\}, \\ \tilde{\mathcal{D}}^e &= \left\{ \boldsymbol{\kappa} \;\middle|\; \sum_{\alpha=1}^{3} \left(\frac{\kappa_\alpha}{\kappa_{c\alpha}} \right)^2 > 1 \right\}, \end{aligned} \tag{3}$$

where κ_m is the minimum wavenumber characterizing the largest represented scale. Note that throughout this paper, Roman letter indices, except for c and f representing coarse and fine respectively, are used for indexed objects that are representing Cartesian vectors and tensors, and in this case the Einstein summation convention applies. On the other hand, Greek indices, c and f are used when indexed objects are not representing Cartesian tensors, and no summation is implied. The other anisotropic wavenumber domain considered here is consistent with a Cartesian tensor product representation of the LES solution in physical space, where the resolution is different in each of the Cartesian basis directions. This Cartesian domain $\mathcal{D}^c$ is defined by

$$\begin{aligned} \mathcal{D}^c &= \{ \boldsymbol{\kappa} \mid \kappa_m < |\kappa_\alpha| \leq \kappa_{c\alpha};\ \alpha = 1,2,3 \}, \\ \tilde{\mathcal{D}}^c &= \{ \boldsymbol{\kappa} \mid |\kappa_\alpha| > \kappa_{c\alpha};\ \alpha = 1,2,3 \}. \end{aligned} \tag{4}$$

This definition of $\mathcal{D}^c$ is anisotropic both because of the Cartesian representation and because the Δ_α are not in general equal. The latter is most significant, and is of primary interest here. An illustrative diagram of the two domain types is provided in Fig. 1.

The Δ_α define an effective resolution cell, essentially a grid cell when using a grid-based numerical representation. We will use the "resolution cell" nomenclature to refer to a volume of the domain with dimensions defined by the Δ_α, even when using numerical methods for which there is no such grid (e.g. spectral methods). Throughout this work, only cell shapes with at least two of the Δ_α equal are considered. These limiting cases are labeled "book" cells (Fig. 2a) when the repeated Δ_α is largest and "pencil" cells (Fig. 2b) when the small Δ_α is repeated. All other cell shapes

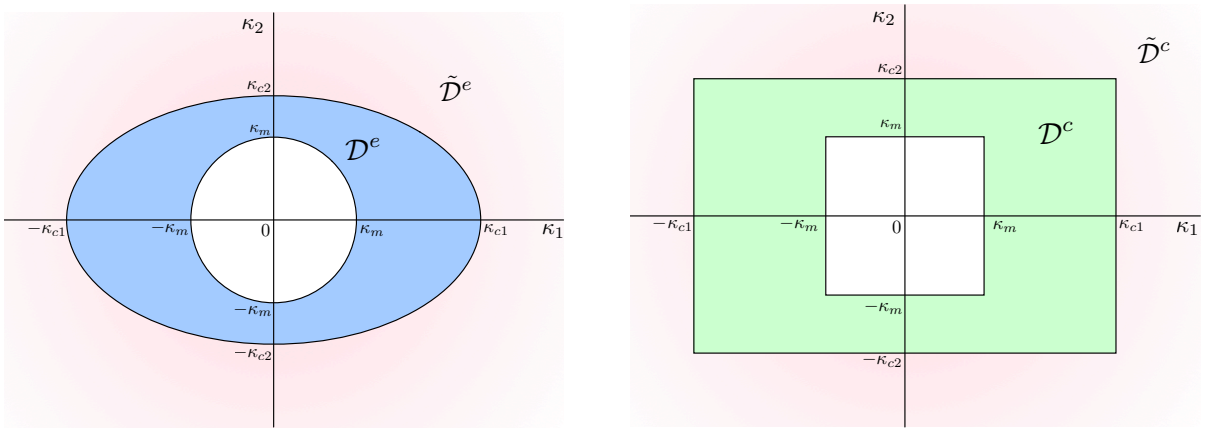

(a) $\mathcal{D}^e$ (b) $\mathcal{D}^c$

FIG. 1. Diagram illustrating 2D representation of (a) ellipsoidal and (b) Cartesian wave-space domain types.

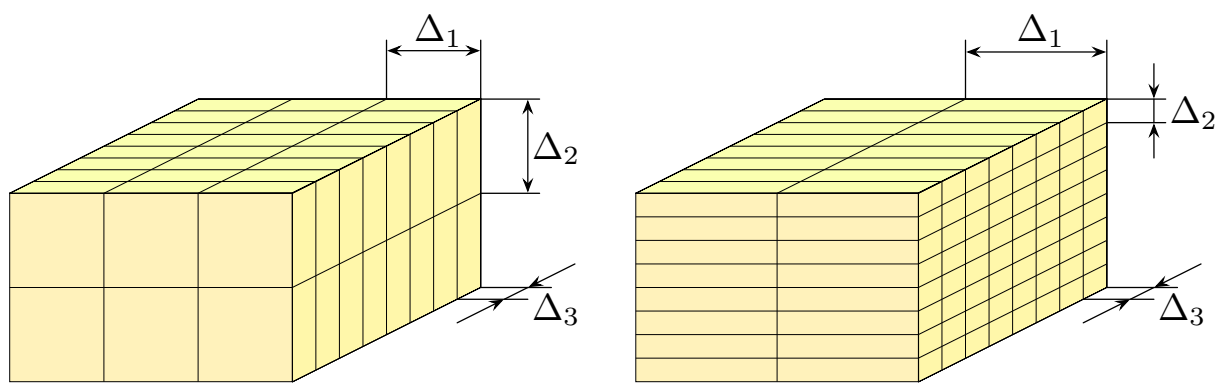

(a) Book (b) Pencil

FIG. 2. Diagram of the limiting (a) book ($\Delta_1 = \Delta_2$) and (b) pencil ($\Delta_2 = \Delta_3$) cell types considered here.

would exhibit behavior intermediate between these cases. These limiting cell shapes are parameterized by the aspect ratio $A_r = \Delta_c/\Delta_f$. Book type cells are particularly common, as they arise naturally to resolve boundary layers. Pencil type cells are typically used more sparingly but are often employed in critical regions such as near stagnation and separation points on 2D bodies.

For isotropic turbulence with anisotropic LES resolution, the unresolved Reynolds stress is weakly anisotropic (Fig. 3a), with anisotropy saturating at A_r of about 32. The saturated level of anisotropy increases with the ratio κ_{cc}/κ_m but since this is occurring as the resolution of the LES is being refined so that the contribution of the unresolved turbulence to the Reynolds stress is becoming negligible, this anisotropy becomes increasing irrelevant to the model [16]. Pencil cells produce significantly more unresolved Reynolds stress anisotropy than book cells. Resolved stress anisotropy (Fig. 3b) similarly saturates at the same A_r and, as expected, is only significant when the smallest κ_{cc}/κ_m approaches one. When $\kappa_{cc}/\kappa_m = 16$ or greater, the resolved anisotropy is negligible. These trends are consistent with those observed by Kaltenbach [9].

If the contribution of unresolved scales to the Reynolds stress were the only relevant function of a SGS model, these

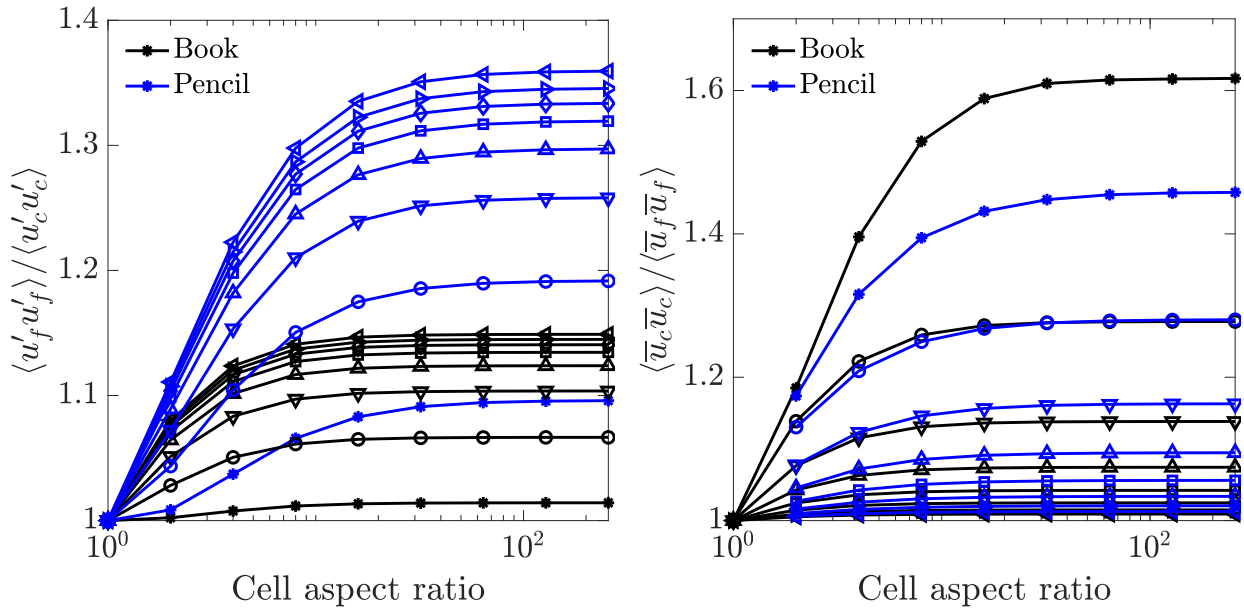

(a) Unresolved (b) Resolved

FIG. 3. Resolution-induced anisotropy in the unresolved (a) and resolved (b) scale contributions to the Reynolds stress for an inertial range energy spectrum, determined as half the trace of (2) and (1), based on the wavenumber domains $\mathcal{D}^e$ and $\tilde{\mathcal{D}}^e$ given by (3). The value of k_{cc}/k_m is 2 *, 4 ∘, 8 ▽, 16 △, 32 □, 64 ◊, 128 ▷, 256 ◁. Subscript "c" indicates the coarse direction while "f" indicates the fine direction.

mild anisotropies would indicate the effects of resolution anisotropy could be neglected. However, as is well known, the primary impact of the unresolved turbulence in well-resolved LES is as a sink of resolved energy. Nearly all subgrid models, which are designed to represent this energy transfer, are formulated in terms of the resolved velocity gradient tensor, so its resolution-induced anisotropy will be important. The energy transfer of an eddy viscosity based subgrid model will necessarily be expressed in terms of second order (or higher) moments of the velocity-gradient tensor. Particularly, if a scalar eddy viscosity is uncorrelated with the velocity gradients, the anisotropy of the energy transfer to the unresolved scales is determined directly from the anisotropy of the second moment of the velocity gradient. Its anisotropy is examined next.

The anisotropy of the second moment of the velocity gradient tensor $\mathcal{G}_{ijkl} = \langle \partial_k \bar{u}_i \partial_l \bar{u}_j \rangle$ induced by anisotropic resolution in isotropic turbulence is calculated by taking the gradient of the spectral energy density tensor twice and again integrating over an anisotropic resolved wavenumber domain $\mathcal{D}$. Noting that $\langle \bar{u}_i \partial_k \partial_l \bar{u}_j \rangle = \langle \partial_k \partial_l \bar{u}_i \bar{u}_j \rangle = 0$, one obtains [15]

$$\mathcal{G}_{ijkl} = \langle \partial_k \bar{u}_i \partial_l \bar{u}_j \rangle = \frac{C_k \varepsilon^{2/3}}{4\pi} \int_{\mathcal{D}} \kappa_k \kappa_l |\boldsymbol{\kappa}|^{-11/3} \left(\delta_{ij} - \frac{\kappa_i \kappa_j}{|\boldsymbol{\kappa}|^2} \right) d\boldsymbol{\kappa}, \tag{5}$$

where $\mathcal{D}$ is again the domain of resolved wavenumbers. The structure of $\mathcal{G}_{ijkl}$ as given in (5) implies that it can be written in terms of a fourth-ranked tensor $\mathcal{A}_{ijkl}$, which is invariant to all permutations of its indices:

$$\mathcal{G}_{ijkl} = \frac{C_k \varepsilon^{2/3}}{4\pi} \left(\delta_{ij} \mathcal{A}_{mmkl} - \mathcal{A}_{ijkl} \right). \tag{6}$$

When the resolved wavenumber domain $\mathcal{D}$ is symmetric about three mutually orthogonal planes through the origin, as is the case for the domains defined in (3) and (4), and the basis in which the tensors are expressed are normal to these symmetry planes, reflection symmetries require that the elements of $\mathcal{G}_{ijkl}$ are zero unless each index is equal to at least one other index, with the same requirements applying to $\mathcal{A}_{ijkl}$. Under these conditions, there are only six distinct non-zero components of $\mathcal{A}$, which can be organized in a symmetric matrix A:

$$\mathcal{A}_{\alpha\alpha\beta\beta} = A_{\alpha\beta} = \int_{\mathcal{D}} \kappa_\alpha \kappa_\alpha \kappa_\beta \kappa_\beta |\boldsymbol{\kappa}|^{-17/3} \, d\boldsymbol{\kappa}. \tag{7}$$

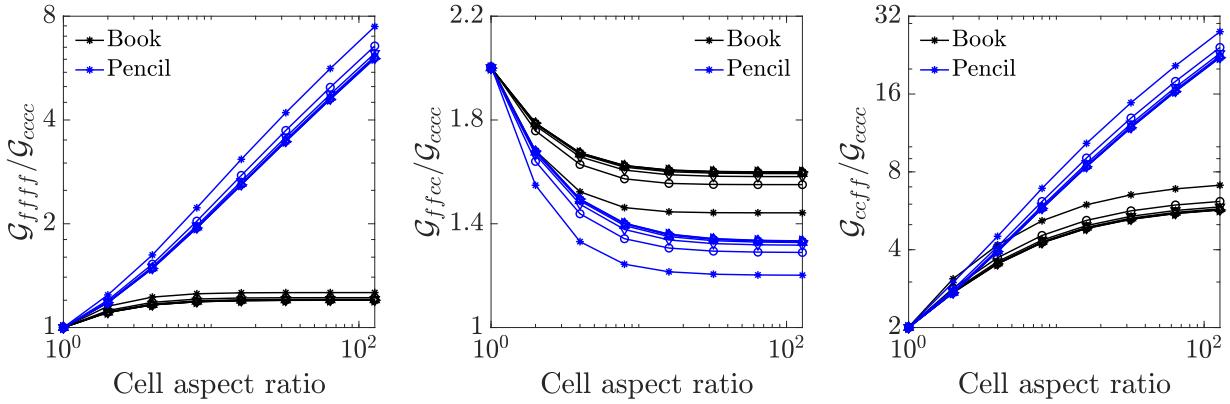

(a) All repeating (b) Fine component, coarse gradient (c) Coarse component, fine gradient

FIG. 4. Resolution-induced anisotropy in the second moment of the resolved velocity gradient tensor $\mathcal{G}_{ijkl}$ determined from (5) based on wavenumber domain $\mathcal{D}^e$ given by (3). The value of k_{cc}/k_m is 2 *, 4 ∘, 8 ▽, 16 △, 32 □, 64 ◊, and 128 ▷. Subscript "c" indicates the coarse direction while "f" indicates the fine direction.

A_r	N_c	N_f	κ_{cc}/κ_m	Cell Types
1	32	32	16	n/a
4	32	128	16	b,p
8	16	128	8	b
8	32	256	16	b,p
8	64	512	32	b
8	128	1024	64	b
16	32	512	16	b,p
32	32	1024	16	b,p

TABLE I. Resolution used in the simulation cases reported here. Listed are the number of Fourier modes in the coarse (N_c) and fine (N_f) directions, for aspect ratios $A_r = N_f/N_c$ ranging from 1 to 32. Simulations were run with book-type cells (indicated with "b") and pencil-type cells ("p"), though not all resolution cases were run with pencil-type cells. The effective resolution in any direction is given by $\Delta_\alpha = L/N_\alpha$, where L is the box size.

In this basis, the remaining components of $\mathcal{A}$ are either zero or equal to those defined in (7), by virtue of the symmetry and invariance properties described above. When the LES resolution is isotropic (i.e. $\mathcal{D}$ is spherically symmetric), each element of A has one of only two distinct values, one for the diagonal elements, and one for the off-diagonal.

In the case of book and pencil cell resolution, where the resolution in two directions is the same, the elements of A include four distinct values. So, the impact of book and pencil cell anisotropic resolution on $\mathcal{G}_{ijkl}$ can be fully described by three ratios of its non-zero elements. These are shown in Fig. 4 as a function of the resolution aspect ratio. Plotted are the ratios $\mathcal{G}_{ffff}/\mathcal{G}_{cccc}$, $\mathcal{G}_{ffcc}/\mathcal{G}_{cccc}$ and $\mathcal{G}_{ccff}/\mathcal{G}_{cccc}$, again, no summation is implied for indices "c" and "f". If $\mathcal{D}$ is isotropic (spherically symmetric), $\mathcal{G}_{ffff}/\mathcal{G}_{cccc}$, $\mathcal{G}_{ffcc}/\mathcal{G}_{cccc}$ and $\mathcal{G}_{ccff}/\mathcal{G}_{cccc}$ have values 1, 2 and 2 respectively. These are the ratios of the variances of the four unique components of the velocity gradient in this situation (i.e. book or pencil cells, with tensors expressed in the grid principle directions). The plots in Fig. 4 show that, as one might expect, the gradients in the fine direction are larger than in the coarse direction, and that they grow relative to the coarse direction derivatives as the aspect ratio increases. For pencil cells the ratios increase like a power between 0.4 and 0.6. These ratios saturate with increasing aspect ratio for book cells. Note that the velocity gradient variances enter the expression for the rate of energy transfer to unresolved scales in the case of a scalar eddy viscosity. So, these quantities represent the contribution to this energy transfer by gradients in the coarse and fine directions.

B. LES Test Cases

A set of large eddy simulations were conducted to test a variety of LES subgrid models with a wide range of of anisotropic resolutions. They consisted of forced homogeneous isotropic turbulence in a cubical periodic domain of size L at infinite Re performed with a modified version of the dealiased pseudo-spectral code *Poongback*[17–19]. Negative

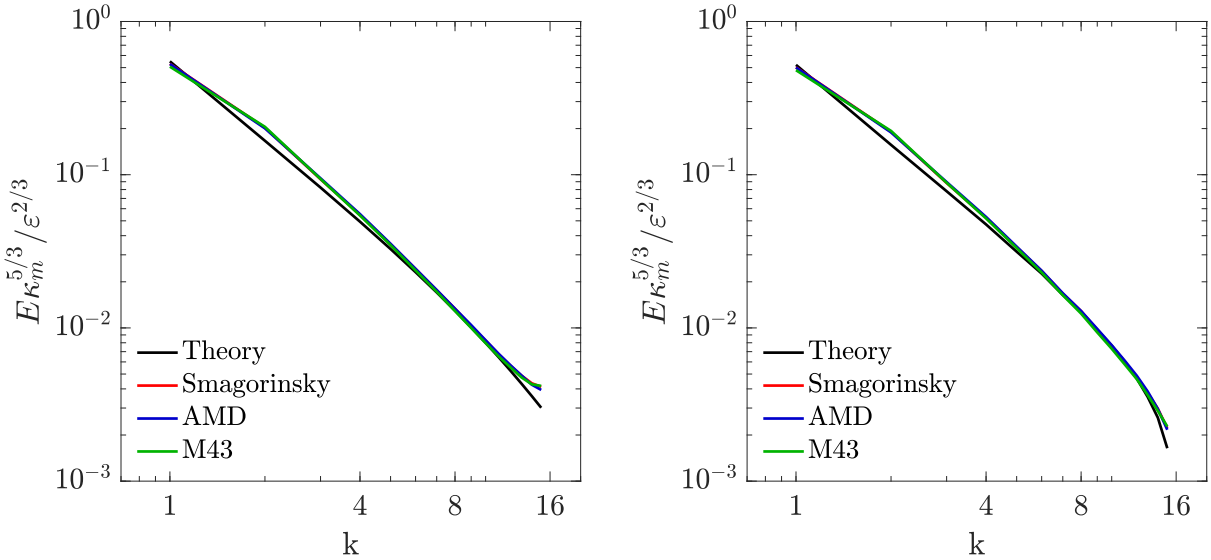

(a) Without spherical filtering

(b) With spherical filtering

FIG. 5. One-dimensional energy spectra E from LES with isotropic resolution using the Smagorinsky, AMD and M43 models, compared with the equivalently filtered $|\boldsymbol{\kappa}|^{-5/3}$ Kolmogorov inertial energy spectra. Shown are spectra (a) without a spherical cut-off filter and (b) with a spherical cut-off filter.

viscosity forcing was used over a band of wavenumbers with magnitudes $|\boldsymbol{\kappa}|L = (0, 4\pi]$ with constant power input. Cell aspect ratios (A_r) range from 1 to 32, as indicated in Table I, which also shows the resolution parameters for each case considered here. Time stepping is performed using low-storage third-order Runge-Kutta [20] with a target maximum $CFL = \pi\Delta t \sum_\alpha (|u_\alpha|/\Delta_\alpha)$, where Δt is the time step. The time step varies in time, so that at step n the time step Δt_n is given by $\Delta t_n = 0.9\Delta t_{n-1} + 0.1\Delta t_{\text{targ}}$ where Δt_{targ} is the time step that would be required to achieve the target maximum CFL. All results presented here are one-dimensional energy spectra [15] normalized by $\kappa_m = 2\pi/L$ and the dissipation ϵ, which is just the specified input forcing power. One-dimensional energy spectra are reported here, instead of the three-dimensional spectra more commonly used for isotropic turbulence, to reveal the differences between the coarsely and finely resolved directions. Spectra are averaged over 10 fields spanning at least four eddy turnover times after being brought to a statistically-stationary state. Throughout the paper, quantities are normalized by ε and κ_m, unless otherwise specified.

Spectra obtained by filtering a theoretical infinite Reynolds number inertial range spectrum are used for comparison to avoid the finite Reynolds number effects inherent in DNS data. This is critical when considering high aspect ratio resolution because the models assume that the resolution scales in all directions are in the inertial range. Comparisons between the LES and the theoretical filtered spectrum are based on ellipsoidal sharp spectral cut-off filters. That is the Fourier transform $\hat{\mathcal{F}}(\boldsymbol{\kappa})$ of the filter kernel is given by:

$$\hat{\mathcal{F}}(\boldsymbol{\kappa}) = \begin{cases} 1 & \text{if } \mathcal{M}_{ij}^2 \kappa_i \kappa_j < \pi^2 \\ 0 & \text{otherwise} \end{cases} \tag{8}$$

Where $\mathcal{M}_{ij}$ is a tensor whose eigenvalues are the grid cell dimensions Δ_α and whose eigenvectors are the grid directions (see Sec. III for more details). This filter excludes all wavenumbers except those in the domain $\mathcal{D}^e$ defined in (3). When simulating isotropic turbulence with anisotropic resolution, such an ellipsoidally filtered turbulence is the most meaningful target of the LES. However, the LES numerical representation and the associated models, are based on a Cartesian tensor product definition of the resolved turbulence ($\mathcal{D}^c$ in Eq. 4). Therefore, to obtain the spectra of interest and compare to the theoretical spectra, the spectral filter defined in (8) is also applied to the LES solutions. Comparisons between LES and theory based on the Cartesian tensor product definition of resolved scales used in the simulations leads to the same conclusions regarding the fidelity of the models as the comparisons reported here.

This is evident in Fig. 5 in which the one-dimensional spectra for cases with $A_r = 1$ are plotted, with and without the spherical truncation that is the isotropic version of the ellipsoidal filter defined above. Shown are results for the three models that are the primary focus of this paper: the Smagorinsky model, the AMD model of [8] and the M43 model presented in Sec. III, compared to the equivalently filtered Kolmogorov inertial range spectrum (labeled

theory). The Smagorinsky constant was adjusted to obtain $C_s = 0.013$ ($\nu_t = C_s\sqrt{2\bar{S}_{ij}\bar{S}_{ij}}\Delta_{eq}^2$) by matching this isotropic resolution case. Similarly, because the numerical representation used here is different from that in [8], the AMD model constant was set to 0.236 to match this case, rather than the suggested value of 0.212 in [8]. Finally, the M43 model constant was determined theoretically (see Appendix A).

In Fig. 5, notice that with or without the spherical truncation, all three models yield nearly identical spectra, including a modest excess of energy at the highest resolved wavenumber, compared to the filtered theoretical spectra, This is manifested as an up-turn in the spectra in the non-spherically-filtered case. All three models perform acceptably well representing the spectra.

C. Smagorinsky model performance with Anisotropic Resolution

The consequences of neglecting resolution anisotropy and the resulting gradient anisotropy can be explicitly demonstrated in LES using the Smagorinsky model [21] applied to simulations with anisotropic resolution. One-dimensional spectra in the fine and coarse directions from such LES are compared to the same obtained from an equivalently filtered $|\boldsymbol{\kappa}|^{-5/3}$ Kolmogorov inertial range (Fig. 6).

For both pencil and book cells, the LES fine-direction spectra have excess energy in the mid wavenumbers centered around the coarse cutoff wavenumber along with a rapid roll-off at high wavenumbers. This high wavenumber energy deficit is most pronounced for book cells. In the coarse-direction spectra, the LES exhibit excess energy at the cutoff, up to a factor of approximately six. This "energy pile-up" at the coarse cutoff appears to be saturating at the highest aspect ratio of 32.

Since the turbulence is homogeneous, this test is insensitive to any errors in representing the subgrid contribution to the Reynolds stress. Therefore, it seems likely that the errors in the energy spectra are purely a result of incorrectly modeling the dissipation anisotropy. This hypothesis is examined later (see Sec. IV B). The results in figure 6 are consistent with expectations for a scalar eddy viscosity when $\mathcal{G}$ is anisotropic due to anisotropic resolution, as discussed above. They show how the resolved turbulence is forced to adjust its energy distribution to accommodate the incorrectly modeled dissipation. For the Smagorinsky model, correlations between the fluctuating eddy viscosity and strain do not correct this overall behavior. With the energy input fixed through low wavenumber stirring, the turbulent field and its gradients must adjust to come into equilibrium and produce a total dissipation equal to the energy injection rate. The deficiencies in the model require that resolved turbulence be distorted to reach this equilibrium, thus the inconsistent spectra. In a more realistic flow scenario, this distortion of the turbulence may have significant consequences. For example, amplifying the energy content near the course grid scale could result in anomalously large turbulent transport, as such lower wavenumbers possess more turbulent kinetic energy. The result would be incorrect prediction of mean quantities. Therefore, here we aspire to pose models that do not distort the resolved turbulence spectra, even in the presence of resolution anisotropy.

Note that using the dynamic approach [1] would not improve these results as the effects of resolution anisotropy would be lost to averaging over all homogeneous directions. Indeed, it has been shown [22] that test filtering should be performed isotropically corresponding to the coarsest grid spacing to obtain decent energy spectra up to the minimum cutoff wavenumber with a large roll-off thereafter when using the dynamic approach and anisotropic grids. It may be possible to construct a tensor-based dynamic coefficient to correct this issue but such an approach has not been explored here. The anisotropy correction of Scotti *et al.* [6] is considered later.

III. A SIMPLE ANISOTROPIC SUBGRID MODEL

To treat resolution anisotropy in subgrid modeling, we begin by relaxing the assumption of an isotropic eddy viscosity, so that the diffusivity can have directional dependence. With an anisotropic eddy viscosity, the standard subgrid model formulation is modified, with the simplest model for the deviatoric portion of the subgrid stress tensor τ_{ij} in terms of a symmetric second rank tensor eddy diffusivity ν_{ij} and the velocity gradient tensor given by

$$-\left(\tau_{ij} - \tfrac{2}{3}k_{sgs}\delta_{ij}\right) \approx \nu_{jk}\partial_k\bar{u}_i + \nu_{ik}\partial_k\bar{u}_j - \tfrac{2}{3}\nu_{lk}\partial_k\bar{u}_l\delta_{ij}, \tag{9}$$

where $k_{sgs} = \frac{1}{2}\tau_{kk}$. Note that the anisotropy of ν_{ij} acts on the derivative components of the gradient tensor, not the velocity components. This is consistent with the fact that the resolution anisotropy introduces anisotropy in scale. Obviously, if ν_{ij} is isotropic, this form reduces to a standard Boussinesq eddy viscosity model. When ν_{ij} is anisotropic, the model for τ_{ij} depends on both the strain rate tensor and the rotation rate tensor, unlike a Boussinesq model.

Second, to support the development of an anisotropic eddy viscosity, we introduce a resolution tensor to express the anisotropy of the resolution. The resolution tensor, $\mathcal{M}_{ij}$, is formally the symmetric part of the Jacobian defining

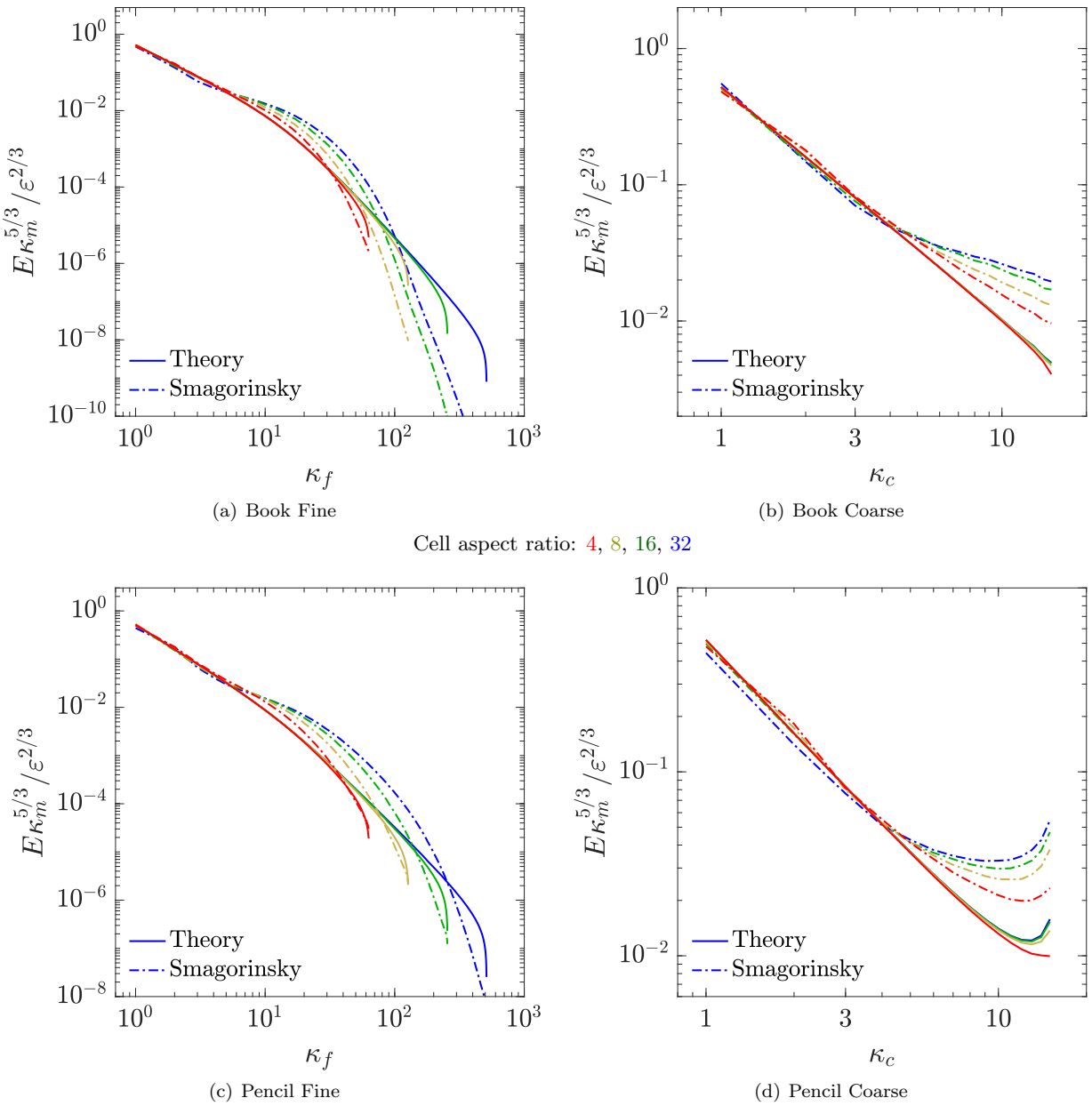

(a) Book Fine (b) Book Coarse

(c) Pencil Fine (d) Pencil Coarse

FIG. 6. One-dimensional energy spectra E, from LES with the standard Smagorinsky model and anisotropic resolution, compared with the equivalently filtered $|\boldsymbol{\kappa}|^{-5/3}$ Kolmogorov inertial range spectra.

the mapping of a unit cube to a resolution cell, or equivalently, the square-root of the cell metric tensor [23]. The eigenvalues $\lambda_i^{\mathcal{M}}$ of $\mathcal{M}_{ij}$ therefore represent the size of a resolution cell in the principal directions while its eigenvectors define those principal directions. Common grid measures are invariants or eigenvalues of $\mathcal{M}_{ij}$; for example,$\Delta_{min} = \min_i \lambda_i^{\mathcal{M}}$, $\Delta_{diag} = (\mathcal{M}_{ij}\mathcal{M}_{ji})^{1/2}$, $\Delta_{vol} = (\det(\mathcal{M}))^{1/3}$, which are the minimum dimension, the diagonal and the cube root of the volume of a resolution cell, respectively. The resolution tensor is a more complete representation of the resolution than scalar measures, so incorporating it into a subgrid model allows the model to retain information about the anisotropy of the resolution. Using a tensor representation of resolution ensures that models constructed from it will be consistent, independent of the orientation of local coordinate systems.

Of primary importance in LES is the LES "dissipation," that is the transfer of energy from the resolved to unresolved scales. Because the LES resolution is anisotropic, variations of resolved velocity in different directions contribute differently to the dissipation. This scale anisotropy of the dissipation can be characterized by the total dissipation

tensor $\hat{\varepsilon}_{ij}$ defined as

$$\hat{\varepsilon}_{ij} = -\tfrac{1}{2}\big(\langle \partial_j \bar{u}_k \tau_{ik}\rangle + \langle \partial_i \bar{u}_k \tau_{jk}\rangle\big). \tag{10}$$

To capture the anisotropic character of this energy transfer, the anisotropic eddy viscosity in the model (9) should satisfy

$$\varepsilon_{ij} = \tfrac{1}{2}\big(\langle \nu_{ik}\partial_j \bar{u}_l \partial_k \bar{u}_l\rangle + \langle \nu_{jk}\partial_i \bar{u}_l \partial_k \bar{u}_l\rangle + \langle \nu_{lk}(\partial_j \bar{u}_l \partial_k \bar{u}_i + \partial_i \bar{u}_l \partial_k \bar{u}_j)\rangle\big) - \tfrac{2}{3}\langle \nu_{lk}\partial_k \bar{u}_l \bar{S}_{ij}\rangle, \tag{11}$$

where $\varepsilon_{ij} = \hat{\varepsilon}_{ij} - \frac{2}{3}\langle k_{sgs}\bar{S}_{ij}\rangle$. This modified dissipation tensor characterizes the contribution of the deviatoric part of the subgrid stress τ, which is the part that the model (9) represents. Further, because of continuity, the isotropic part of τ does not contribute to the dissipation, so that the dissipation $\varepsilon = \hat{\varepsilon}_{ii} = \varepsilon_{ii}$. The simplest possible anisotropic eddy viscosity model is one in which the eddy viscosity does not fluctuate, so that in (11) it can be moved out of the expected value, resulting in

$$\varepsilon_{ij} = \tfrac{1}{2}\big(\nu_{ik}\mathcal{G}_{lljk} + \nu_{jk}\mathcal{G}_{llik} + \nu_{lk}(\mathcal{G}_{lijk} + \mathcal{G}_{ljik})\big) - \tfrac{1}{3}\nu_{lk}(\mathcal{G}_{jkil} + \mathcal{G}_{ikjl}). \tag{12}$$

Furthermore, in isotropic turbulence, all anisotropy arises due to the anisotropy of resolution. Therefore, the tensors ε_{ij}, ν_{ij} and $\mathcal{M}_{ij}$ must all have the same eigenvectors and for the Cartesian tensor product filtering used here, these are just the coordinate basis. In this basis, ε_{ij} and ν_{ij} are diagonal with the eigenvalues $\lambda^{\varepsilon}_{\alpha} = \varepsilon_{\alpha\alpha}$ and $\lambda^{\nu}_{\alpha} = \nu_{\alpha\alpha}$ on the diagonals, and $\mathcal{G}_{ijkl}$ has the characteristics described in Sec. II. This allows the α eigenvalue λ^{ν}_{α} of ν_{ij} to be determined in terms of the eigenvalues $\lambda^{\varepsilon}_{\alpha}$ of ε_{ij} by solving the following coupled system of three linear equations

$$\lambda^{\varepsilon}_{\alpha} = \lambda^{\nu}_{\alpha}\mathcal{G}_{jj\alpha\alpha} + \sum_{\beta}\lambda^{\nu}_{\beta}\mathcal{G}_{\beta\alpha\alpha\beta} - \tfrac{2}{3}\sum_{\beta}\lambda^{\nu}_{\beta}\mathcal{G}_{\alpha\beta\alpha\beta}. \tag{13}$$

The resulting anisotropic eddy viscosity is *a priori* consistent with the scale anisotropy of the dissipation ε_{ij}. Unfortunately, while we have an evaluation of $\mathcal{G}_{ijkl}$ from inertial range theory, we have no such simple evaluation for ε_{ij}. A model for the three-point third-order correlation has been formulated [24], and in principle it could be used to develop a representation for ε_{ij} for a given definition of the resolved turbulence, but that is out of scope of the current paper. Instead, we consider the form of the model relevant for isotropic resolution, and use its form as a guide to generalizing to anisotropic resolution.

When $\mathcal{D}$ is spherically symmetric including wavenumbers with magnitudes ranging from κ_m to κ_c, the integral in (5) can be performed over spheres to obtain

$$\mathcal{G}_{\alpha\alpha\alpha\alpha} = \tfrac{4}{5}C_k\varepsilon^{2/3}\big(\kappa_c^{4/3} - \kappa_m^{4/3}\big) \tag{14}$$

which, due to isotropy and the constraints described in Sec. II, completely determines the κ_c dependence of $\mathcal{G}_{ijkl}$. All other components are proportional to $\mathcal{G}_{\alpha\alpha\alpha\alpha}$, with the constant of proportionality depending on the component. Therefore the solution of (13) in this case must be

$$\lambda^{\nu} = C\varepsilon^{1/3}(\kappa_c^{4/3} - \kappa_m^{4/3})^{-1}, \tag{15}$$

where C is a constant, which in principle is determined in terms of C_k, and $\nu_{ij} = \lambda^{\nu}\delta_{ij}$ is isotropic. Since $\kappa_c = \pi/\Delta$ with $\Delta = \lambda^{\mathcal{M}}$ and $\kappa_m = 2\pi/L$ with L either the domain size or proportional to the integral scale, a consistent generalization to anisotropic resolution is

$$\lambda^{\nu}_{\alpha} = C(\hat{\mathcal{M}})\varepsilon^{1/3}((\lambda^{\mathcal{M}}_{\alpha})^{-4/3} - (L/2)^{-4/3})^{-1}, \tag{16}$$

where now $C(\mathcal{M})$ generally depends only on the invariants of the scaled resolution tensor $\hat{\mathcal{M}} = \mathcal{M}/\Delta$, where $\Delta = \min_i \lambda^{\mathcal{M}}_i$; that is, only on the anisotropy of $\mathcal{M}$. If the $\lambda^{\mathcal{M}}$ are sufficiently small compared to L, then the L term can be neglected yielding the basic M43 model

$$\nu_{ij} = C(\hat{\mathcal{M}})\varepsilon^{1/3}\mathcal{M}_{ij}^{4/3}. \tag{17}$$

The tensor eddy viscosity in (17) is essentially an anisotropic extension of the "Kolmogorov expression" model [25, 26]. The dependence on $\mathcal{M}^{4/3}$ is consistent with diffusivity anisotropy scaling with face-normal grid dimension to the 4/3, as in [13]. Also, Bardina *et al* [11] proposed, but did not pursue, what amounts to a tensor diffusivity model, where the diffusivity is a general tensor function of the cell moment of innertia tensor ($\mathcal{M}^2$). Diffusivity anisotropy that scales with $\mathcal{M}^{4/3}$ is therefore a special case of this dependence, provided the coefficients in the Bardina formulation

are taken to be functions of the invariants of the cell moment of innertia tensor. When the $\lambda^{\mathcal{M}}$ are not small enough compared to L, the more general "low-k" version, consistent with (16) is obtained by replacing $\mathcal{M}$ in (17) with a modified resolution tensor $\mathcal{M}^*$ given by

$$\mathcal{M}^*_{ij} = (\mathcal{M}^{-4/3} - (L/2)^{-4/3}\mathcal{I})^{-3/4}_{ij} \tag{18}$$

The coefficient $C(\mathcal{M})$ is determined by requiring that when applied to the filtered theoretical spectrum the model dissipates energy at the rate ε (see Appendix A). Thus, the coefficient is determined theoretically in terms of the Kolmogorov constant C_k, consistent with the filter and numerical representation used in the LES. This is similar to the theoretical determination of the Smagorinsky constant as in [27, 28], except that unlike those previous theoretical estimates, the theoretical constants determined here produce very good results (see Sec. IV). The difference is that in the M43 model used here, the eddy diffusivity does not fluctuate (see Sec. IV B). Also provided in Appendix A is a fit used here to represent the functional dependence of C on the eigenvalues of $\mathcal{M}$. Consistent with the Fourier spectral representation used in the LES, $C(\mathcal{M})$ is determined here based on $\mathcal{G}$ computed on the $\mathcal{D}^c$ domain defined in (4).

IV. MODEL TESTS

In this section, the proposed M43 model, its low-k variant and the AMD model of [8] are tested in detail in infinite Reynolds number LES of isotropic turbulence with anisotropic resolution. For the modified Smagorinsky model of Scotti [6] and the Vreman model [7], which also include a dependence on the resolution anisotropy, a high-aspect ratio example is included to demonstrate that they exhibit similar deficiencies as the basic Smagorinsky model (Fig. 6).

The AMD model and a subtle technical issue related to its formulation are discussed briefly in Appendix B. Here we note that as written in [8] (equation 23), the model is tensorially inconsistent. However, it can be recast in terms of the resolution tensor $\mathcal{M}$ to be tensorially consistent, while being equivalent to the formulation in [8] for rectilinear grids with the grid cells aligned with the coordinate directions (see Appendix B). It is this recast form of AMD that we evaluate here.

Note that the AMD model and the M43 model described in Sec. III are fundamentally different. The M43 model poses a tensor eddy viscosity (16) with the only flow-dependence being the expected value of the kinetic energy dissipation, ε . In homogeneous turbulence, ε is not spatially varying and in the statistically stationary flows considered here, it is not time dependent either. Therefore, the viscosity tensor is a single constant tensor specified entirely *ab initio*. In contrast, the AMD model uses a scalar eddy viscosity with a non-linear dependence on the local velocity gradient along with local clipping, and is therefore strongly spatially dependent and discontinuous. With these stark differences, it is remarkable that these two models produce energy spectra that are so similar.

A. One-dimensional energy spectra

As with the Smagorinsky model evaluated in Sec. I, models are assessed based on their ability to predict the one-dimensional energy spectra when performing an LES of infinite Reynolds number forced homogeneous isotropic turbulence with anisotropic resolution (see Fig. 7-11). All the models considered here yield virtually identical results for isotropic resolution (see Fig. 5).

We begin by performing the same book and pencil cell evaluations up to aspect ratios of 32 as for the Smagorinsky model (Fig. 6). The AMD model results are shown in Fig. 7 with M43 shown in Figures 8. Both of these models perform quite well in comparison to Smagorinsky (Fig. 6) with little energy pile-up at the cutoff in the coarse direction. In the AMD model, there is a very small excess of energy in the coarse spectrum, especially toward the cutoff with pencil cells, which rapidly saturates with increasing aspect ratio. With the M43 model, there is apparent over-dissipation in wavenumbers near the cutoff primarily in fine directions for both cell types resulting in reduced spectral energy near the cutoff. This behavior appears to increase with cell aspect ratio. The AMD model also produces spectra that are too low near the cutoff in the fine direction, though the character of the curves is more complex. Particularly, the spectra roll off with a slope that is not monotonically increasing with wavenumber.

To explore the effect of scale separation between the largest turbulent scales and the coarsest filter cutoff, we examine model performance as a function of the ratio of the coarsest cutoff wavenumber, κ_{cc}, to minimum resolved wavenumber, κ_m, with a fixed cell aspect ratio of 8 for book cells. In the cases considered, the integral scale L_{int} is given by $L_{int}\kappa_m \approx 1.38$, so varying κ_{cc}/κ_m similarly varies $L_{int}\kappa_{cc}$. Shown in figure 9 are spectra for $\kappa_{cc}/\kappa_m = 8$, 16, 32 and 64. In addition to the M43 model in both its basic and low-k version and AMD, the Smagorinsky model is evaluated for reference (Fig. 9(a)). The previously observed pileup of energy near the coarse cutoff for Smagorinsky

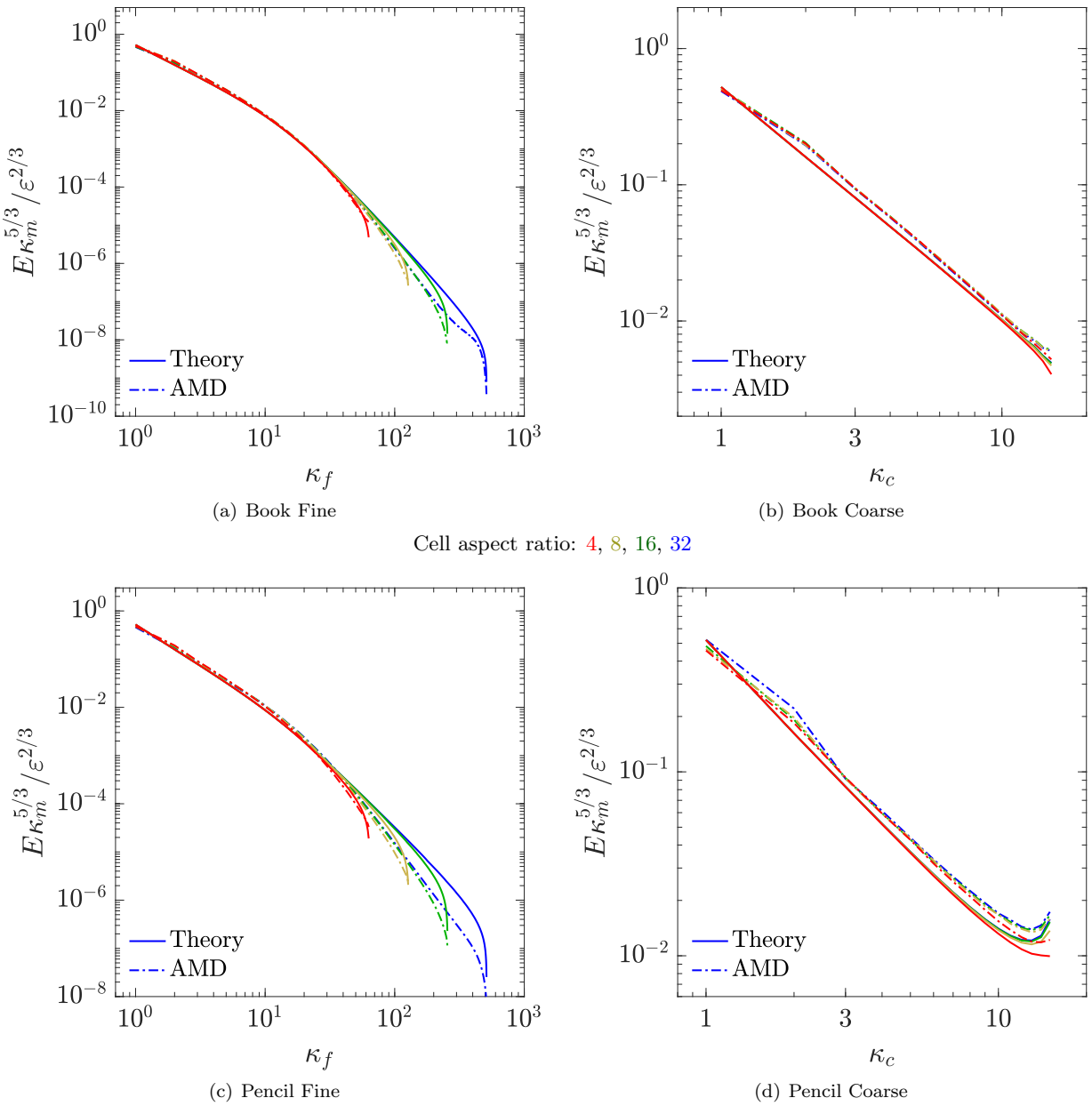

(a) Book Fine (b) Book Coarse

(c) Pencil Fine (d) Pencil Coarse

FIG. 7. One-dimensional energy spectra E from LES with the AMD model and anisotropic resolution, compared with the equivalently filtered $|\boldsymbol{\kappa}|^{-5/3}$ Kolmogorov inertial energy spectra.

increases relative to the total resolved energy as κ_{cc}/κ_m is reduced. Once again, the M43 models and AMD vastly out-perform Smagorinsky and yield nearly the theoretical spectra. The low-k version of the M43 model is virtually indistinguishable from the basic M43, even for $\kappa_{cc}/\kappa_m = 8$. It my be that the low-k correction will be important for smaller values of κ_{cc}/κ_m, though it is clearly not for the cases considered here.

Finally, we briefly discuss the Vreman model [7] (Fig. 10) and the Scotti modification of Smagorinsky [6] (Fig. 11). For both models, the qualitative performance is similar to Smagorinsky, with energy pile up at the coarse direction cutoff and mid-range of the fine direction, while the energy is low near the fine direction cutoff. As the Vreman model was primarily designed to cause the model viscosity to vanish in laminar regions, poor results in the presence of anisotropic grids is not surprising. However, we have considered the Vreman model here because it is one of the very few SGS models which directly incorporates grid anisotropy into its formulation through the weighting of velocity gradients with directional grid length scales. These poor results show how simple gradient weighting alone is not

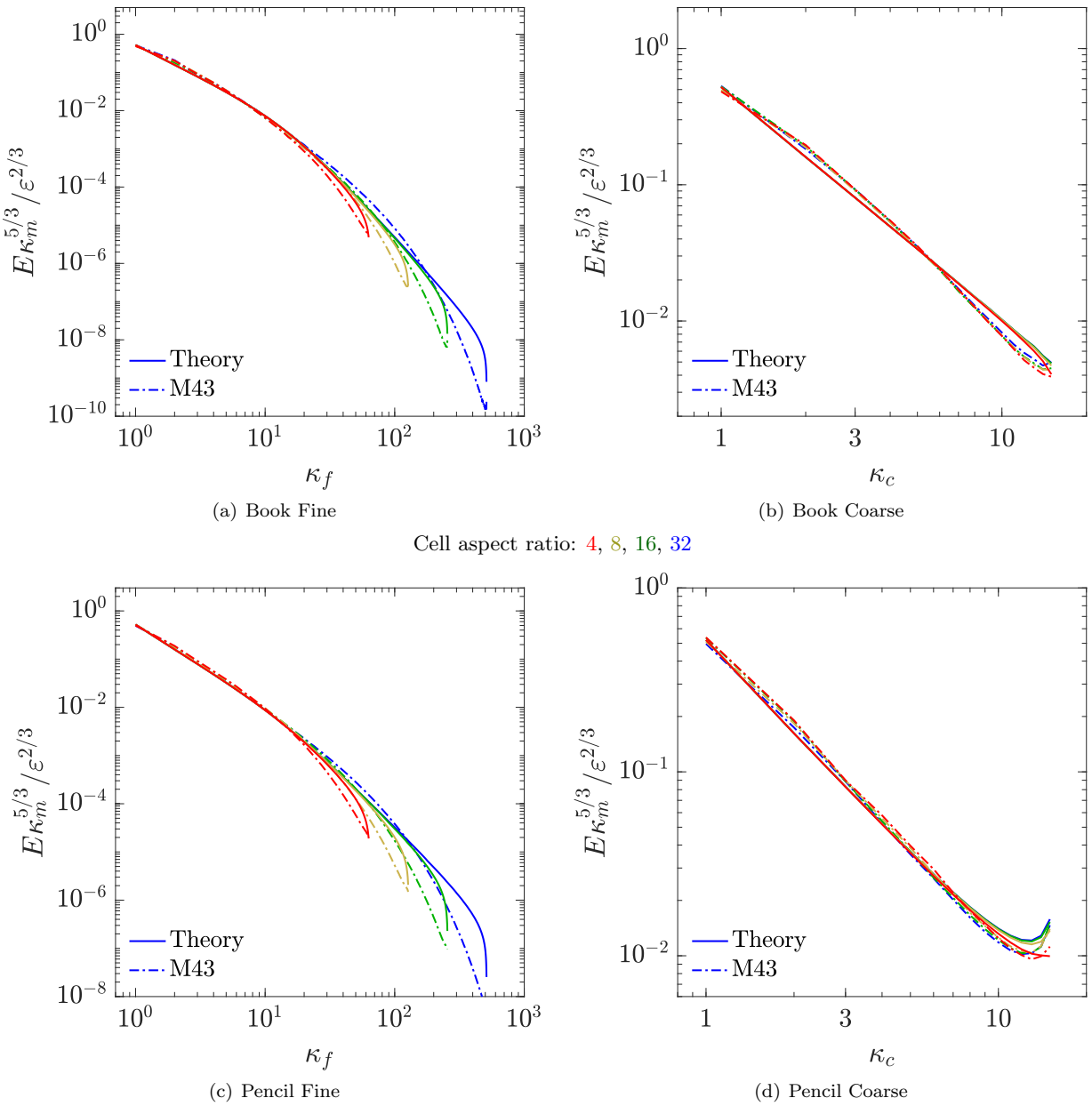

(a) Book Fine (b) Book Coarse

(c) Pencil Fine (d) Pencil Coarse

FIG. 8. One-dimensional energy spectra E from LES with the M43 model and anisotropic resolution, compared with the equivalently filtered $|\boldsymbol{\kappa}|^{-5/3}$ Kolmogorov inertial energy spectra.

sufficient to correct issues caused by anisotropic grids. Scotti's modified Smagorinsky effectively increases the model constant in response to the cell aspect ratio. Naturally, it cannot improve the anisotropic resolution behavior of the Smagorinsky model and can only reduce coarse direction energy pile-ups by increasing the eddy diffusivity. This is precisely the observed behavior. However, especially for pencil cells, it appears the correction should be enhanced, as there continues to be excessive energy at the cutoff in the coarse direction. Energy spectra resulting from both the Vreman and modified Smagorinsky highlight that modifying the model constant is not sufficient to address resolution anisotropy; rather, an appropriate model structure is necessary.

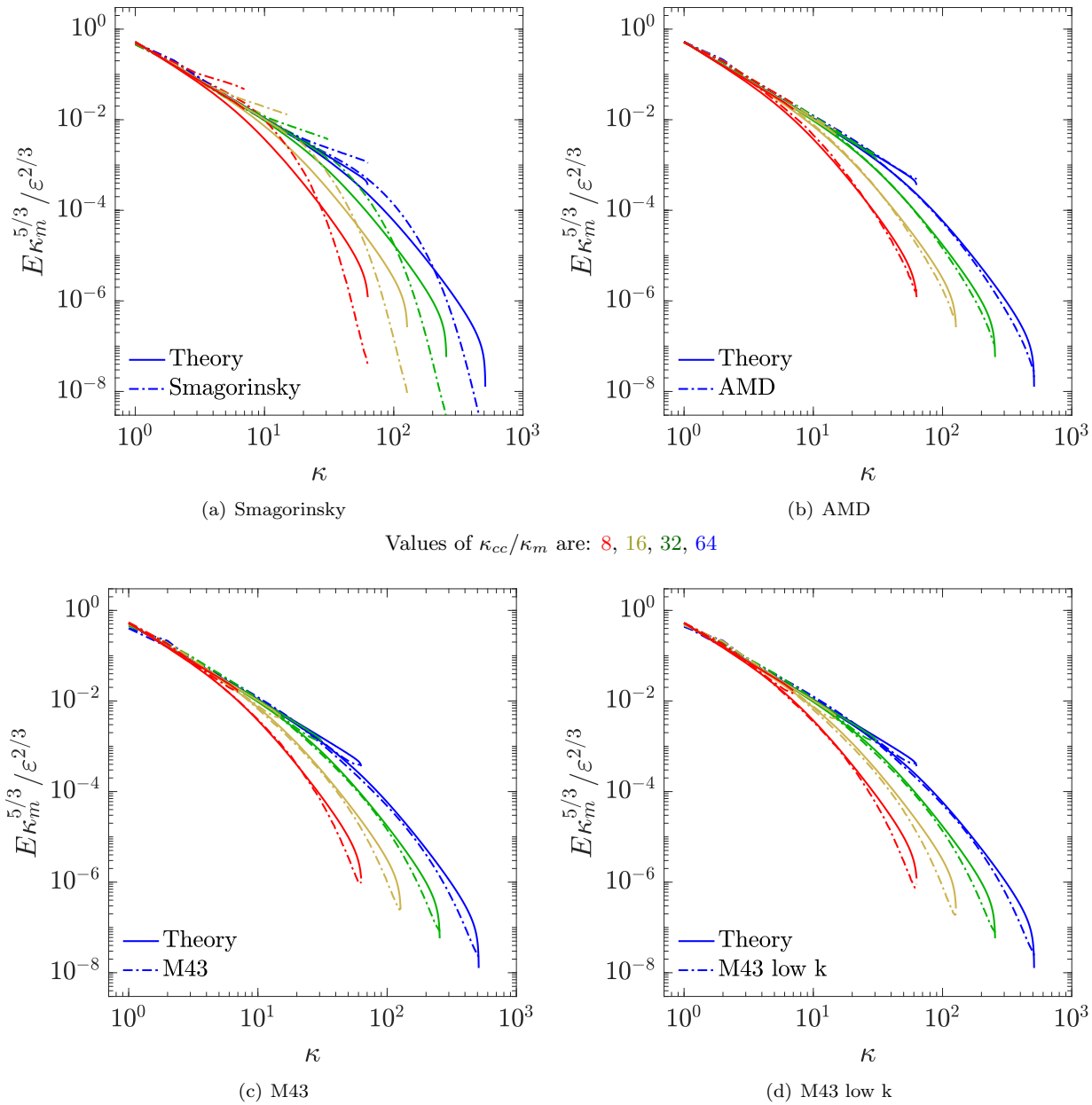

(a) Smagorinsky (b) AMD

Values of κ_{cc}/κ_m are: 8, 16, 32, 64

(c) M43 (d) M43 low k

FIG. 9. One-dimensional energy spectra E from LES for book cells using the Smagorinsky, AMD, M43 and M43 low-k models and anisotropic resolution with $A_r = 8$ and varying values of κ_{cc}/κ_m, compared with the equivalently filtered $|\boldsymbol{\kappa}|^{-5/3}$ Kolmogorov inertial energy spectra. Shown are spectra in both the fine and coarse directions.

B. Dissipation anisotropy

Both the M43 model and the AMD model perform notably well on the anisotropic resolution cases studied here, despite the prominent differences in their formulation. This raises the question as to what they have in common that other models lack that leads to the good performance on these tests. An obvious candidate for this shared feature is the anisotropic energy transfer to small scales (10), which measures the contributions of stress and velocity gradients in different directions to the energy transfer. In light of (11), it seems probable that this directional contribution to energy transfer should have a direct impact on the one dimensional spectra studied in Sec. IV A, and indeed the importance of this energy transfer tensor was assumed in the formulation of the M43 model (Sec. III). To test this hypothesis, ε_{ij} was computed from the LES presented in Sec. IV A using the M43, AMD, and Smagorinsky models as

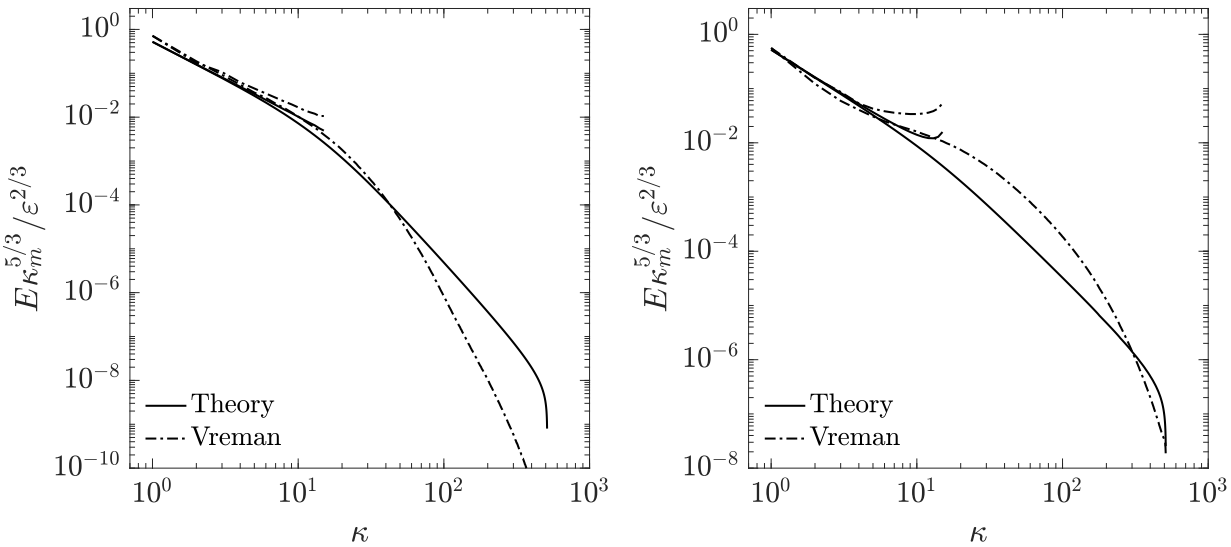

(a) Book (b) Pencil

FIG. 10. One-dimensional energy spectra E from LES with the Vreman model [7] with $C_v = 0.07$ and anisotropic resolution of aspect ratio 32, compared with the equivalently filtered $|\boldsymbol{\kappa}|^{-5/3}$ Kolmogorov inertial energy spectra. Shown are spectra in both the fine and coarse directions.

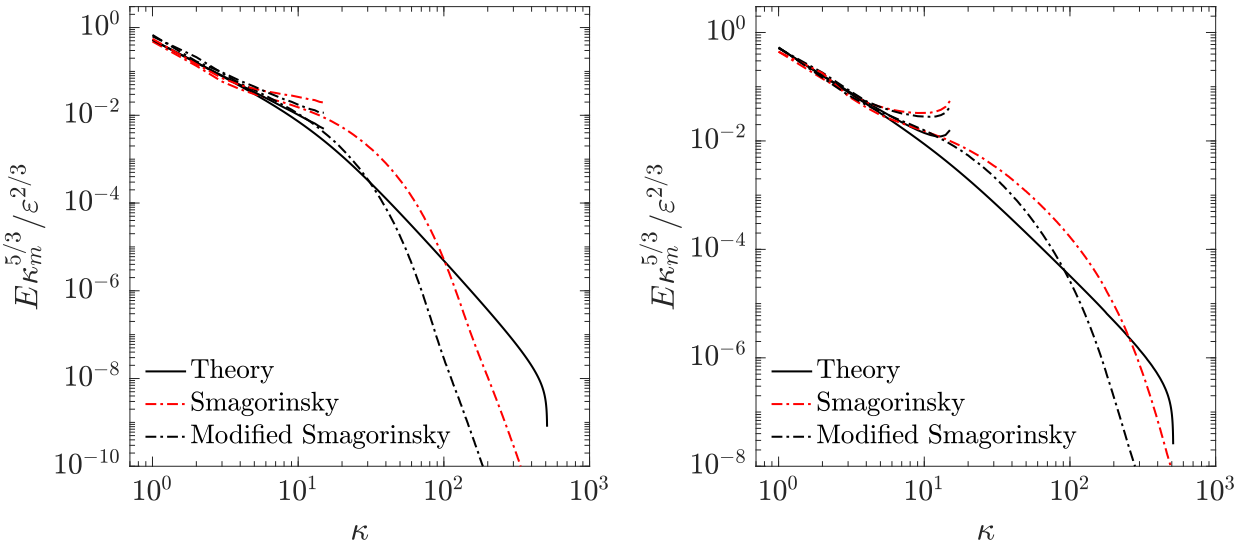

(a) Book (b) Pencil

FIG. 11. One-dimensional energy spectra E from LES with the Smagorinsky model and the modified Smagorinsky model of Scotti [6], using anisotropic resolution with aspect ratio 32, compared with the equivalently filtered $|\boldsymbol{\kappa}|^{-5/3}$ Kolmogorov inertial energy spectra. Shown are spectra in both the fine and coarse directions.

a function of resolution aspect ratio. Because the turbulence being simulated is isotropic, the only source of anisotropy is the resolution. This guarantees that ε_{ij} has the same eigenvectors as $\mathcal{M}$, regardless of model. Further, because the LES are (isotropically) forced and stationary, the total energy transfer ε_{ii} is just the mean rate at which energy is introduced by the forcing, which is also the same regardless of model. Therefore, to compare ε_{ij} for the different models, it suffices to compare it's eigenvalues λ^{ε} normalized by ε_{ii}. To this end, the normalized eigenvalues associated with eigenvectors in the coarse and fine resolution directions are shown as a function of aspect ratio in Fig. 12.

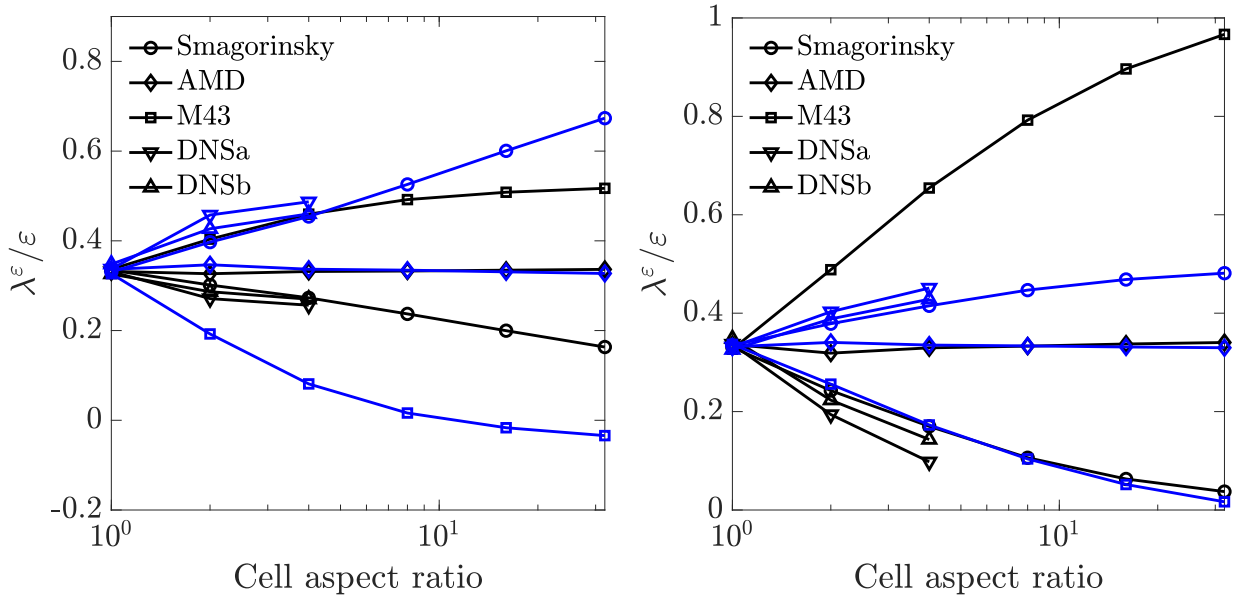

(a) Book (b) Pencil

FIG. 12. Normalized values of the gradient direction ε_{ij} (10) eigenvalues as a function of cell aspect ratio in LES with $\kappa_{cc}/\kappa_m = 16$ using the Smagorinsky, AMD, and M43 models. Also shown are values from a filtered DNS with equivalent forcing and $Re_\lambda = 205$ performed with 512^3 Fourier modes. The filters used on the DNS were consistent with LES resolution with $\kappa_{cc}/\kappa_m = 16$ (DNSa) and $\kappa_{cc}/\kappa_m = 8$ (DNSb). Black lines represent λ_c^ϵ and blue lines represent λ_f^ϵ.

The results shown in Fig. 12 are surprising. For both book and pencil cells, the energy transfer with the M43 model is dominated by gradients in the coarse direction(s). For book cells, this trend is so pronounced that for aspect ratio greater than 16, the contribution of gradients in the fine direction become slightly negative, that is representing net energy transfer from small to large scales. The Smagorinsky results are exactly the opposite with gradients in the fine direction(s) dominating the energy transfer. When using the AMD model, ε_{ij} is much closer to isotropic, with the coarse and fine direction eigenvalues nearly the same, resulting in normalized values of about a third.

Equivalently filtered 512^3 DNS ($Re_\lambda = 205$, $\kappa_c\eta = 1.5$) with identical forcing is also plotted using filters with $\kappa_{cc}/\kappa_m = 16$, as in the LES, labeled "DNSa" in Fig. 12, and with $\kappa_{cc}/\kappa_m = 8$, labeled "DNSb" in Fig. 12, to reduce finite Reynolds number effects. The definition of ε_{ij} and therefore $\varepsilon = \varepsilon_{ii}$ does not include resolved viscous dissipation. Obviously, this is zero in our infinite Reynolds number LES, but it is not zero in the DNS. The resolved viscous contribution is larger in the case with $\kappa_{cc}/\kappa_m = 16$ resulting in somewhat elevated anisotropy in this normalized statistic. While the dissipation contribution of DNS does not match any model particularly well, it does most closely resemble that of the Smagorinsky model with the fine directions contributing the most. The fact that both the AMD and M43 models perform well with anisotropic resolution, but produce strikingly different anisotropic characteristics of ε_{ij} from both each other and DNS shows that reproducing this statistic is not necessary for capturing the anisotropy of the resolved spectrum. To further explore the issue, we next examine component-wise dissipation anisotropy.

While the dissipation tensor in (10) is contracted over component indices, the actual modeled dissipation appearing in the resolved Reynolds stress transport equation is contracted over gradient indices. Thus, the dissipation tensor expressed as

$$\tilde{\varepsilon}_{ij} = -\tfrac{1}{2}\big(\langle \partial_k \bar{u}_j \tau_{ik}\rangle + \langle \partial_k \bar{u}_i \tau_{jk}\rangle\big). \tag{19}$$

is another natural candidate to explore to help identify the statistical conditions that are necessary for good model performance. These results are shown in Fig. 13.

Unlike the directional-anisotropy, the component-wise dissipation anisotropy for M43 is qualitatively consistent with DNS. Again, none of the models match the DNS curves in Fig. 13 exactly, however, the two DNS filter cases bound the M43 dissipation anisotropy for both cell types. For both book and pencil cells, the energy transfer with the M43 model is dominated by the velocity components corresponding to the fine direction(s). The Smagorinsky results are again exactly the opposite with components of the coarse direction(s) dominating the energy transfer. And again, the AMD model is much closer to isotropic. While the M43 dissipation anisotropy has saturated for book cells and

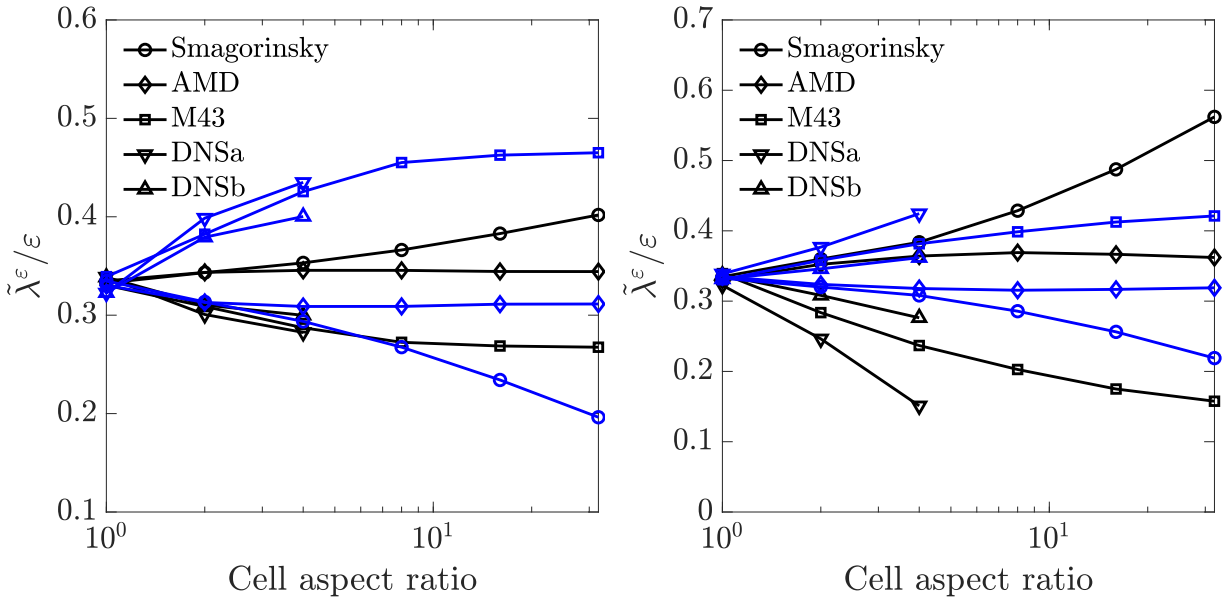

(a) Book (b) Pencil

FIG. 13. Normalized values of component-wise ε_{ij} (19) eigenvalues as a function of cell aspect ratio in LES with $\kappa_{cc}/\kappa_m = 16$ using he Smagorinsky, AMD, and M43 models. Also shown are values from a filtered DNS with equivalent forcing and $Re_\lambda = 205$ performed with 512^3 Fourier modes. The filters used on the DNS were consistent with LES resolution with $\kappa_{cc}/\kappa_m = 16$ (DNSa) and $\kappa_{cc}/\kappa_m = 8$ (DNSb). Black lines represent λ_c^ϵ and blue lines represent λ_f^ϵ.

appears to be nearly so for pencil cells, Smagorinsky anisotropy continues to increase with A_r. Furthermore, the sense of the anisotropy (i.e. whether coarse or fine eigenvalues are larger) arising from the AMD and Smagorinsky models is opposite that of the DNS and M43 model. Whether this is important may depend on the ultimate purpose of the simulation. However, the fact that both the AMD and M43 models perform well with anisotropic resolution, but produce strikingly different $\tilde{\varepsilon}_{ij}$ anisotropies, shows that reproducing this statistic is also not necessary for capturing the anisotropy of the resolved spectrum.

Given the importance of the dissipation to the spectral dynamics, representing the directional and/or component-wise dissipation anisotropy would seem to be a requirement for generating the correct energy spectra. That it is not is quite curious and motivates future examination of the particular correlations present in the AMD model that allow it to perform well despite not representing these seemingly critical statistic. In the case of M43, it is plausible to suppose that its good performance is a direct result of representing the true component-wise dissipation statistic. If true, while reproducing $\tilde{\varepsilon}_{ij}$ is not necessary in general, it may be so for non-fluctuating eddy viscosities. Without the correlations of a fluctuating eddy viscosity to introduce anisotropy, the model must represent relevant anisotropies of the dissipative processes directly by construction. At least for HIT with anisotropic resolution, this construction appears to be relatively straight-forward, resulting in the M43 model reported here.

C. Non-fluctuating eddy viscosity

One of the interesting things about the M43 model presented here is that the eddy viscosity does not fluctuate. As in some of the models studied in [26], the eddy viscosity is considered a mean quantity. This has some clear advantages that arise from the fact that it makes analyzing the model much easier because one does not need to consider correlations between a fluctuating eddy viscosity and the fluctuating velocity gradient. However, with isotropic resolution, the M43 model has a scalar eddy viscosity, and an LES with a non-fluctuating scalar eddy viscosity would appear to be a DNS at some low Reynolds number. That this is not so is a consequence of the limited resolution used to represent the turbulent fluctuations, as suggested by [29]. In the M43 model, the eddy viscosity was determined to ensure that when the model is applied to turbulence with a Kolmogorov inertial range extending up to the spectral resolution cutoff, that it will dissipate energy at the rate ε. This means simply that the subgrid model dissipation does not preclude a truncated $\kappa^{-5/3}$ spectrum as the LES solution. Whether this is realized or

not depends on the details of the energy transfer among scales in the LES. This is distinctly different from a DNS in which the resolution is sufficient to capture the viscous roll off of the spectrum. With isotropic resolution, the M43 eddy viscosity leads to an effective "Kolmogorov scale" $\eta_e \approx 0.136\Delta$ so that the effective $k_c\eta_e \approx 0.428$. This is much smaller than that considered adequate resolution for DNS (e.g. $k_c\eta \geq 1.5$ in [30]).

All the other models considered here use a fluctuating eddy viscosity, and the question arises as to whether the fluctuations contribute to the veracity of the model. It is at least plausible that a fluctuating eddy viscosity could better represent the scale dependent transfer of energy to unresolved scales, leading to a better representation of the the truncated spectrum or perhaps other statistics. However, as shown in Fig. 5, LES with isotropic resolution using the Smagorinsky, AMD and M43 models yield almost identical results. It appears then, at least for the energy spectra, the fluctuations of the eddy viscosity in the Smagorinsky and AMD models do not improve the veracity of the model when applied to LES with isotropic resolution. This is consistent with the observations in [26] regarding the Smagorinsky model applied to decaying isotropic turbulence. However, from Sec. IV A, the fluctuating eddy viscosity does allow the AMD model to treat anisotropic resolution without resorting to an anisotropic eddy viscosity, though this is not true for the Smagorinsky and Vreman models.

V. DISCUSSION AND CONCLUSIONS

Application of LES in complex geometries, or even just wall bounded flows, will generally involve grids with anisotropic resolution. Even when the turbulence is isotropic, anisotropic LES resolution results in resolved and unresolved turbulence that are anisotropic, violating the isotropic unresolved scales assumption underlying many subgrid models, and as a result common LES models perform poorly (Secs. II and IV A). One consequence of resolution anisotropy is that the resolved velocity gradient tensor is strongly anisotropic, while the subgrid contribution to the mean Reynolds stress is only mildly so. One therefore cannot expect a scalar eddy viscosity to correctly represent the latter in general. A potential method to correct this deficiency is to construct an eddy viscosity that is uncorrelated with the gradient fluctuations so that its contribution to the mean stress only acts through the mean gradients [31]. This is another sense in which eddy viscosity subgrid models are ill-suited to representing the unresolved mean Reynolds stress, as first observed by Jimenez & Moser [16].

Treatment of resolution anisotropy in LES has been largely neglected. The one existing model that does effectively treat resolution anisotropy is the AMD model introduced in [8], which uses a scalar eddy viscosity and performs well on our tests. In addition, we here introduced a new subgrid model formulation to treat resolution anisotropy based on a second rank tensor eddy viscosity (Sec. III). This model performs similarly to the AMD model in producing the correct anisotropic spectra in our simulations of isotropic turbulence with anisotropic resolution. However, the AMD and M43 models could not be more different, and considering these differences and the fact that they do not result in significant performance differences yields a number of insights into what is important about an LES model, at least for representing resolution anisotropy.

First, consider that the only flow-dependence in the M43 model is the mean rate of kinetic energy dissipation, as in the Kolmogorov scaled model in [26]. It is necessary that an eddy viscosity produce the correct dissipation, as has been widely understood, which makes an explicit model dependence on the dissipation rate natural. Indeed, one interpretation of the dynamic Smagorinsky model [1], is that the dynamic procedure serves to ensure that the dissipation rate is consistent [16]. Since the M43 eddy viscosity depends only on mean quantities, it only varies in space and time on the scale of mean variations, not on the scale of the resolved fluctuations. This is unlike virtually every other LES model, including AMD, in which the eddy viscosity fluctuates with the resolved turbulent fluctuations. The good performance of the M43 model shows that, at least in the case of HIT, it is not necessary for an LES eddy viscosity to fluctuate or depend on fluctuating resolved quantities, consistent with observations of [26], and the presence of eddy viscosity fluctuations appears to be of no utility in the Smagorinsky model.

Clearly, the mechanisms by which the AMD and M43 models represent resolution anisotropy are completely different. For M43, the representation is direct with the anisotropy of a tensor eddy viscosity determined directly from the anisotropy of the resolution tensor (17). In contrast, the AMD model has a scalar eddy viscosity so that the anisotropic characteristics of the model arise entirely from the anisotropic correlation of the fluctuating eddy viscosity with the resolved velocity gradients. It is not clear why this should work so well for anisotropic resolution in the AMD model. The AMD modeling ansatz of setting the eddy viscosity to an estimate of the minimum required to dissipate the variance of the velocity gradient at the rate that it is produced does not appear to speak to this correlation characteristic. So while the M43 model developed here is constructed specifically to perform well with anisotropic resolution, the good AMD performance just arose in a model developed based on other considerations. For future model refinement and development, it would be useful to determine the characteristics of AMD that lead to this good performance.

Also of interest is the fact that the *a posteriori* anisotropy of the directional and component energy transfer tensors,

ε_{ij} and $\tilde{\varepsilon}_{ij}$ as defined in (10) and (19), are essentially different between LES performed with M43 and AMD models. Since these tensors characterize the contributions of different gradient directions and velocity components to the transfer of energy to the unresolved scales, they would seem to be critical to the dynamics of the resolved scales. While representing $\tilde{\varepsilon}_{ij}$ may be sufficient for the M43 model to perform well in our tests, the results in Sec. IV A show that correctly representing these quantities in an LES is not necessary for good representation of the spectra. This raises the question of what statistical characteristics of the subgrid model are necessary for good performance with anisotropic resolution and anisotropic turbulence in general. Knowing this would allow the design of models with these characteristics.

Finally, we note that the M43 model proposed here has some features to recommend it beyond the relatively good performance for LES with anisotropic resolution. One is that the model, in theory, has no adjustable constants, or rather, the model constant is determined in terms of the Kolmogorov constant. The constant appearing in (17), which is a function of $\mathcal{M}$ can be determined from the Kolmogorov inertial range spectrum, and characteristics of the numerical derivative operators and filter type (Appendix A). The M43 model parameterized this way yields the correct resolved spectra, as shown in Sec. IV A. This is possible because the M43 eddy viscosity does not fluctuate. However, the M43 model and its parameterization could fail to represent the correct spectrum if the resolved scales are not in a Kolmogorov inertial range, because the Reynolds number is too low. It would be interesting to explore whether a finite Reynolds number analysis as in [28] could be generalized to anisotropic resolution to produce a low Reynolds number version of M43.

Another useful feature of the M43 model is that it is formulated directly in terms of the mean rate of energy transfer to the unresolved scales (ε). This might appear to be a liability, since ε is not generally known *a priori*. However, because it is a well-defined scalar statistical quantity that at high Reynolds number is independent of the scale at which it is determined, it can be naturally found dynamically. Indeed, Dantinne *et.al.*[26] did precisely this for the the equivalent of the isotropic version of the M43 model. Alternatively, if one is carrying equations for the dissipation, as for example in a hybrid RANS/LES formulation, that dissipation can be used [32].

APPENDIX A: M43 COEFFICIENT

Let $\mathbb{G}$ be the normalized version of $\mathcal{G}$ as defined in (20); that is,

$$\mathbb{G}_{ijkl} = \mathcal{G}_{ijkl}\varepsilon^{-2/3}\Delta_{min}^{4/3} \tag{20}$$

where Δ_{min} is the minimum eigenvalue of the resolution tensor, $\mathcal{M}$. The normalized tensor (20) then depends only on the scaled resolution tensor $\hat{\mathcal{M}} = \mathcal{M}/\Delta_{min}$. For isotropic turbulence, we can evaluate (20) numerically for a wide range of resolution anisotropies by assuming a Kolmogorov inertial range resulting in the scaled version of (5). This calculation of $\mathbb{G}$ can account for the use of numerical approximations of derivatives in computing the velocity gradients in an LES, and the implicit or explicit filter defining the LES. This is accomplished by introducing the effective wavenumber $\hat{\boldsymbol{\kappa}}(\boldsymbol{\kappa})$ for the numerical approximation of the first derivatives into (5), and applying the homogeneous filter operator to the integrand, yielding

$$\mathbb{G}_{ijkl} = \frac{C_k\Delta_{min}^{4/3}}{4\pi}\int_{\mathcal{D}} \hat{\kappa}_k\hat{\kappa}_l\mathcal{F}^2(\boldsymbol{\kappa})|\boldsymbol{\kappa}|^{-11/3}\left(\delta_{ij} - \frac{\kappa_i\kappa_j}{|\boldsymbol{\kappa}|^2}\right)d\boldsymbol{\kappa}, \tag{21}$$

where $\mathcal{F}$ is the filter operator. For example, when a finite volume (box) filter is used, $\mathcal{F}(\boldsymbol{\kappa}) = \Pi_{i=1}^3\mathrm{sinc}(\kappa_i\lambda_i^{\mathcal{M}}/2)$. For the LES performed here using the spectral numerical method in *PoongBack*, $\hat{\boldsymbol{\kappa}} = \boldsymbol{\kappa}$ and $\mathcal{F} = 1$. Consistent with the numerical representation in *PoongBack*, the domain of integration is the Cartesian domain $\mathcal{D}^c$ defined in (4). The minimum wavenumber is $\kappa_m = 2\pi/L$, where L is the domain size, and the cutoff wavenumbers in each of the principle directions of $\mathcal{M}$ are $\kappa_{c\alpha} = \pi/\lambda_\alpha^{\mathcal{M}}$, where as in Sec. III, $\lambda_\alpha^{\mathcal{M}}$ is the αth eigenvalue of $\mathcal{M}$. Reexpressing (4) in these terms yields:

$$\mathcal{D} = \mathcal{D}^c = \{\boldsymbol{\kappa}|\kappa_m \leq |\boldsymbol{\kappa}\cdot\boldsymbol{\phi}_\alpha^{\mathcal{M}}| < \kappa_{c\alpha};\ \alpha = 1,2,3\}, \tag{22}$$

where $\boldsymbol{\phi}_\alpha^{\mathcal{M}}$ is the unit eigenvector of $\mathcal{M}$ associated with $\lambda_\alpha^{\mathcal{M}}$. In a more general setting (other than turbulence in a periodic box), the large scale L would be proportional to the integral scale. For any $\mathcal{M}$, when expressed in the Cartesian basis defined by the eigenvectors of $\mathcal{M}$, (21) is non-zero only when each index value is repeated.

For a given resolution anisotropy, the model coefficient $C(\hat{\mathcal{M}})$ in (17) is determined to ensure that the eddy viscosity tensor will produce the specified dissipation, and likewise for $C^*(\hat{\mathcal{M}}^*)$ for the low-k version of the model. To this

	M43	M43 low-k
$C^{\circ}_{\mathcal{M}}$	0.0700	0.0700
c_{00}	0.9091	0.9091
c_{10}	0.2733	0.2738
c_{01}	0.0199	0.0185
c_{20}	−0.0312	−0.0316
c_{11}	−0.1472	−0.1472
c_{02}	0.0200	0.0188
c_{30}	−0.0038	−0.0037
c_{21}	0.0201	0.0201
c_{12}	−0.0028	−0.0030
c_{03}	0.0207	0.0202
c_{40}	0.0007	0.0007
c_{31}	−0.0007	−0.0007
c_{22}	0.0012	0.0012
c_{13}	0.0017	0.0017
c_{04}	0.0035	0.0034

TABLE II. Values of the fitting coefficients in (25) based on $\mathcal{G}$ computed with $L/\lambda^{\mathcal{M}}_{max} = 64$ for the M43 and M43 low-k models. The value of $C^{\circ}_{\mathcal{M}}$ was determined from (24).

end the eddy viscosity model (17) is substituted into the trace of the expression for the dissipation tensor (11). Since $\varepsilon_{ii} = \varepsilon$, the result can be solved for C, yielding

$$C(\hat{\mathcal{M}}) = \left(\hat{\mathcal{M}}^{4/3}_{jk}\mathbb{G}_{lljk} + \hat{\mathcal{M}}^{4/3}_{jk}\mathbb{G}_{lljk} + \hat{\mathcal{M}}^{4/3}_{lk}(\mathbb{G}_{ljjk} + \mathbb{G}_{ljjk})\right)^{-1} \tag{23}$$

and the same expression is used to evaluate $C^*(\hat{\mathcal{M}}^*)$, by substituting $\hat{\mathcal{M}}^*$ for $\hat{\mathcal{M}}$ in (23). There remains only a single free constant, the Kolmogorov constant C_k, that enters the model of $\mathcal{G}$ in (5). The overall model constant ($C^{\circ}_{\mathcal{M}}$ below) is calculated by considering the isotropic resolution case in the limit where $\kappa_c \gg \kappa_m$. In this case $\hat{\mathcal{M}} = \mathcal{I}$, the identity, and (23) simplifies to

$$C^{\circ}_{\mathcal{M}} = C(\mathcal{I}) = \frac{4\pi\Delta^{4/3}_{min}}{C_k}\left(\int_{\mathcal{D}} 2|\boldsymbol{\kappa}|^{-5/3}\,d\boldsymbol{\kappa}\right)^{-1} = \frac{2}{C_k\pi^{1/3}}\left(8\int_{\tilde{\mathcal{D}}}|\tilde{\boldsymbol{\kappa}}|^{-5/3}\,d\tilde{\boldsymbol{\kappa}}\right)^{-1} \approx \frac{0.1106}{C_k} \tag{24}$$

where the domain $\tilde{\mathcal{D}}$ is the unit cube with one vertex at the origin. Taking $C_k \approx 1.58$ as found in [30] yields $C(\mathcal{I}) \approx 0.070$, which is used here. This is about 1.5% lager than the value found by calibrating an LES with isotropic resolution to match the filtered theoretical spectrum as closely as possible, which yields only slight improvements in the spectrum. It appears that 1.5% is well within the uncertainty in the Kolmogorov constant.

By setting $C^{\circ}_{\mathcal{M}}$ in this way, one essentially determines the magnitude of the eddy viscosity that is *necessary* for resolved-scale turbulence with a Kolmogorov inertial-range spectrum to dissipate at the required rate. This can be exact because the eddy viscosity does not fluctuate, unlike with similar estimates for Smagorinsky as in [27, 28]. Of course, setting the M43 constant thus does not guarantee that the LES will produce a Kolmogorov inertial range, but if it does not, it is not the fault of the eddy viscosity magnitude being set incorrectly. There are a number of issues that could lead to poor representation of the spectra, such as dissipative and/or dispersive numerics or the distortions of nonlinear interactions due to the truncation implied by the filter or projection. However, with this model and non-dissipative numerics, it is *not possible* to correct for such errors by adjusting the magnitude of the eddy viscosity. As shown in Sec. IV A, for the dealiased pseudo-spectral numerics (no dissipation or dispersion) and the Fourier truncation projections used here, the M43 model with the constant $C(\mathcal{M})$ determined theoretically in this way *does* result in a good representation of Kolmogorov inertial range spectra, over a wide range of resolution characteristics.

Since C is a scalar, it can only depend on the eigenvalues of $\hat{\mathcal{M}}$, and since by construction one of those eigenvalues is one, this is a two dimensional function. It can be evaluated for a wide range of resolution anisotropies characterized by the ratio of the eigenvalues of $\mathcal{M}$ to its minimum eigenvalue. A fit of this function is described below.

Without loss of generality, let $\lambda^{\mathcal{M}}_3$ be the smallest eigenvalue of $\mathcal{M}$ and $\lambda^{\mathcal{M}}_1$ the largest. Then $C(\mathcal{M})$ depends only on $\lambda^{\hat{\mathcal{M}}}_1 > \lambda^{\hat{\mathcal{M}}}_2 \geq 1$. Let $r^2 = (\lambda^{\hat{\mathcal{M}}}_1)^2 + (\lambda^{\hat{\mathcal{M}}}_2)^2$ and let $\theta = \cos^{-1}(\lambda^{\hat{\mathcal{M}}}_1/r)$, where $0 \leq \theta \leq \pi/4$. The function $C(\mathcal{M})$ is

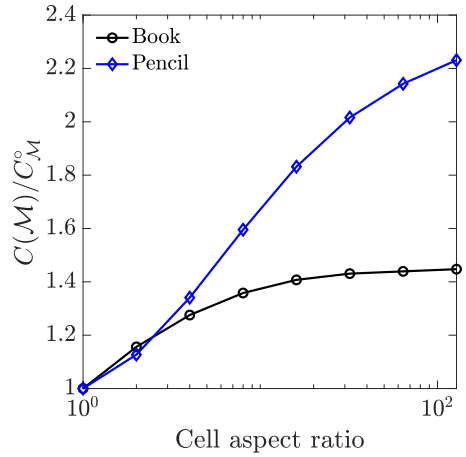

FIG. 14. Normalized coefficients for the basic M43 model as a function of cell aspect ratio using (25). All other cell types fall in between book and pencil limiting cases.

then fit as a quadratic function of $x = \ln(r)$ and $y = \ln(\sin(2\theta))$. That is:

$$C(\mathcal{M}) \approx C^{\circ}_{\mathcal{M}} \sum_{i=0}^{4} \sum_{j=0}^{4-i} c_{ij} x^i y^j \tag{25}$$

Here the values of c_{ij} are normalized so that for isotropic resolution ($r = \sqrt{2}$, $\theta = \pi/4$), the sum in (25) is 1, and then $C^{\circ}_{\mathcal{M}} = C(\mathcal{I})$ as determined above. For the M43 simulations performed here, fits including aspect ratios up to 128 were performed for spectral numerics with $\mathcal{G}$ computed with $L/\lambda_1^{\mathcal{M}} = 64$. This is large enough for the dependence on L to be weak (see figure 4). The resulting values of c_{ij} are given in table II, and the values of $C(\mathcal{M})/C^{\circ}_{\mathcal{M}}$ for book and pencil resolution are plotted in figure 14.

APPENDIX B: MODIFIED AMD MODEL

The AMD model was introduced by Rozema *et al.* [8]. It was evaluated in Sec. IV and found to perform remarkably well on isotropic turbulence LES with anisotropic resolution. However, there is a technical detail in the formulation of the model that needs be addressed, which is discussed briefly here.

The expression $(\delta x_i \partial_i v_j)(\delta x_i \partial_i v_j)$ is introduced in equation (18) of [8], and similar expressions are used throughout the subsequent development. Here δx_i is the size of the rectangular filter box in the i direction (the grid size in the i direction of a Cartesian grid) and $\partial_i v_j$ is the velocity gradient tensor. The expression $\delta x_i \partial_i$ is described in [8] as the scaled gradient operator. Throughout the paper, Cartesian tensor notation and the Einstein summation convention are employed. However the expression above and those like it throughout the paper are not valid Cartesian tensor expressions because the index i appears four times. As a consequence, the meaning of the expression is ambiguous, but from context and by comparison to the QR model development, it is clear that what is meant is

$$(\delta x_i \partial_i v_j)(\delta x_i \partial_i v_j) = \sum_{i=1}^{3} (\delta x_i \partial_i v_j)(\delta x_i \partial_i v_j). \tag{26}$$

The reason this cannot be expressed in a valid Cartesian tensor expression is that the directional filter sizes δx_i, do not make up a tensorially valid vector. In essence, (26) can only make sense when the Cartesian basis vectors are normal to the faces of the filter box.

This difficulty can be addressed by observing that the δx_i are actually the eigenvalues of the resolution tensor $\mathcal{M}$ introduced in Sec. III, and in the case of rectangular filter boxes, the eigenvectors of $\mathcal{M}$ are normal to the faces of the box. A tensorially consistent representation of the scaled gradient is then $\mathcal{M}_{ik}\partial_k$, and the expression in (26) is written

$$\sum_{i=1}^{3} (\delta x_i \partial_i v_j)(\delta x_i \partial_i v_j) = (\mathcal{M}_{ik}\partial_k v_j)(\mathcal{M}_{il}\partial_l v_j). \tag{27}$$

In (27), the left hand expression is valid only in the the special Cartesian basis normal to the filter box faces, while the right hand expression is valid generally and is equivalent to the left hand expression in this special basis.

We point this generalization out here for two reasons. First is that a valid model must be tensorially consistent, and so it is important that there is a tensorially consistent expression of the AMD model. Second, using the tensorially consistent version of the AMD model allows it to be applied in a broader set of circumstances. The generalized AMD model expression for the eddy viscosity ν_e (equation 23 in [8]) is given by

$$\mathcal{R}_{ij} = (\mathcal{M}_{km}\partial_m v_i)(\mathcal{M}_{kn}\partial_n v_j), \tag{28}$$

$$\nu_e = C\frac{\max(-\mathcal{R}_{ij}S_{ij}, 0)}{(\partial_k v_j)(\partial_k v_j)}, \tag{29}$$

which is obtained by pushing the generalize scaled gradient through the development that leads to equation (23) in [8].

ACKNOWLEDGMENTS

The authors acknowledge the generous financial support from the National Aeronautics and Space Administration (cooperative agreement number NNX15AU40A), the Air Force Office of Scientific Research (grant FA9550-11-1-007) and the Exascale Computing Project (17-SC-20-SC), a collaborative effort of two U.S. Department of Energy organizations (Office of Science and the National Nuclear Security Administration). Thanks are also due the Texas Advanced Computing Center at The University of Texas at Austin for providing HPC resources that have contributed to the research results reported here (`http://www.tacc.utexas.edu`).

[1] M. Germano, U. Piomelli, P. Moin, and W. H. Cabot, A dynamic subgrid-scale eddy viscosity model, Physics of Fluids A: Fluid Dynamics **3**, 1760 (1991).
[2] D. K. Lilly, A proposed modification of the germano subgrid scale closure method, Physics of Fluids A: Fluid Dynamics **4**, 633 (1992).
[3] U. Piomelli and E. Balaras, Wall-layer models for large-eddy simulations, Annual Review of Fluid Mechanics **34**, 349 (2002).
[4] J. Larsson, S. Kawai, J. Bodart, and I. Bermejo-Moreno, Large eddy simulation with modeled wall-stress: recent progress and future directions, Bulletin of JSME **3** (2016).
[5] S. T. Bose and G. I. Park, Wall-modeled large-eddy simulation for complex turbulent flows, Annual Review of Fluid Mechanics **50**, 535 (2018).
[6] A. Scotti, C. Meneveau, and D. K. Lilly, Generalized Smagorinsky model for anisotropic grids, Physics of Fluids A **5**, 2306 (1993).
[7] A. Vreman, An eddy-viscosity subgrid-scale model for turbulent shear flow, Physics of Fluids **16**, 3670 (2004).
[8] W. Rozema, H. J. Bae, P. Moin, and R. Verstappen, Minimum-dissipation models for large-eddy simulation, Physics of Fluids **27**, 085107 (2015).
[9] H.-J. Kaltenbach, Cell aspect ratio dependence of anisotropy measures for resolved and subgrid scale stresses, Journal of Computational Physics **136**, 399 (1997).
[10] J. W. Deardorff, A numerical study of three-dimensional turbulent channel flow at large reynolds numbers,, Journal of Fluid Mechanics **41**, 453 (1970).
[11] J. Bardina, J. H. Ferziger, and W. C. Reynolds, Improved aubgrid scale models for large eddy simulation, AIAA 13th Fluid and Plasma Dynamics Conference **AIAA-80-1357** (1980).
[12] U. Schumann, Subgrid scale model for finite difference simulations of turbulent flows in plane channels and annuli, Journal of Computational Physics **18**, 374 (1975).
[13] S. Zahrai, F. H. Bark, and R. I. Karlsson, On anisotropic subgrid modeling, European Journal of Mechanics B **14**, 459 (1995).
[14] R. Verstappen, When does eddy viscosity damp subfilter scales sufficiently?, J. Sci. Comput. **49**, 94 (2011).
[15] S. B. Pope, *Turbulent Flows* (Cambridge University Press, 2000).
[16] J. Jiménez and R. D. Moser, Large-eddy simulations: Where are we and what can we expect?, AIAA Journal **28**, 605 (2000).
[17] M. Lee, N. Malaya, and R. D. Moser, Petascale direct numerical simulation of turbulent channel flow on up to 786K cores, in *the International Conference for High Performance Computing, Networking, Storage and Analysis* (ACM Press, New York, New York, USA, 2013) pp. 1–11.

[18] M. Lee, R. Ulerich, N. Malaya, and R. D. Moser, Experiences from Leadership Computing in Simulations of Turbulent Fluid Flows, Computing in Science Engineering **16**, 24 (2014).

[19] M. Lee and R. D. Moser, Direct numerical simulation of turbulent channel flow up to Re=5200, Journal of Fluid Mechanics **774**, 395 (2015).

[20] P. R. Spalart, R. D. Moser, and M. M. Rogers, Spectral methods for the Navier-Stokes equations with one infinite and two periodic directions, Journal of Computational Physics **96**, 297 (1991).

[21] J. Smagorinsky, General circulation experiments with the primitive equations. i. the basic experiment, Mon. Weather Rev. **91**, 99 (1963).

[22] A. Scotti, C. Meneveau, and M. Fatica, Dynamic smagorinsky model on anisotropic grids, Physics of Fluids **9** (1996).

[23] J. L. Synge and A. Schild, *Tensor Calculus* (Dover, 1949) pp. 26–30.

[24] H. Chang and R. D. Moser, An inertial range model for the three-point third-order velocity correlation, Physics of Fluids **19** (2007).

[25] D. Carati, K. Jansen, and T. Lund, A family of dynamic models for large-eddy simulation, CTR Annual Research Briefs (1995).

[26] G. Dantinne, H. Jeanmart, G. S. Winckelmans, V. Legat, and D. Carati, Hyperviscosity and vorticity-based models for subgrid scale modeling, Applied Scientific Research **59**, 409 (1998).

[27] K. Lilly, *On the application of the eddy viscosity concept in the inertial sub-range of turbulence*, Tech. Rep. Manuscript 123 (National Center for Atmospheric Research, 1966).

[28] C. Meneveau and T. S. Lund, The dynamic Smagorinsky model and scale-dependent coefficients in the viscous range of turbulence, Physics of Fluids **9**, 3932 (1997).

[29] O. Thiry, G. Winckelmans, and M. Duponcheel, The dynamic Smagorinsky model in 512^3 pseudo-spectral LES of decaying homogeneous isotropic turbulence at very high Re_λ, in *Direct and Large-Eddy Simulation XI*, edited by M. V. Salvetti, V. Armenio, J. Fröhlich, B. J. Geurts, and H. Kuerten (Springer, 2019) pp. 123–128.

[30] D. A. Donzis and K. R. Sreenivasan, The bottleneck effect and the Kolmogorov constant in isotropic turbulence, J. Fluid Mech. **657**, 171 (2010).

[31] J. C. Uribe, N. Jarrin, R. Prosser, and D. Laurence, Development of a two-velocities hybrid RANS-LES model and its application to a trailing edge flow, Flow Turbulence Combust **85**, 181 (2010).

[32] S. Haering, T. Oliver, and R. D. Moser, Towards a predictive hybrid RANS/LES framework, AIAA Scitech 2019 Forum **AIAA 2019-0087** (2018).